Histone H1 prevents non-CG methylation-mediated small RNA biogenesis in *Arabidopsis* heterochromatin

Jaemyung Choi[1,#], David B. Lyons[1,#], and Daniel Zilberman[1,2,*]

[1]Department of Cell and Developmental Biology, John Innes Centre, Norwich, UK

[2]Institute of Science and Technology, Klosterneuburg, Austria

[#]These authors contributed equally to this work

*Correspondence: daniel.zilberman@ist.ac.at

Abstract

Flowering plants utilize small RNA molecules to guide DNA methyltransferases to genomic sequences. This RNA-directed DNA methylation (RdDM) pathway preferentially targets euchromatic transposable elements. However, RdDM is thought to be recruited by methylation of histone H3 at lysine 9 (H3K9me), a hallmark of heterochromatin. How RdDM is targeted to euchromatin despite an affinity for H3K9me is unclear. Here we show that loss of histone H1 enhances heterochromatic RdDM, preferentially at nucleosome linker DNA. Surprisingly, this does not require SHH1, the RdDM component that binds H3K9me. Furthermore, H3K9me is dispensable for RdDM, as is CG DNA methylation. Instead, we find that non-CG methylation is specifically required for small RNA biogenesis, and without H1 small RNA production quantitatively expands to non-CG methylated loci. Our results demonstrate that H1 enforces the separation of euchromatic and heterochromatic DNA methylation pathways by excluding the small RNA-generating branch of RdDM from non-CG methylated heterochromatin.

Introduction

Transposable elements (TEs) and their remnants comprise a substantial fraction of eukaryotic genomes and generally must be kept silent to ensure genome integrity and function (Bourque et al., 2018). TE silencing is achieved despite the disruption caused by each cell division, whereby half of the genome and histone proteins are made anew. Robust cellular memory of the inactive state is achieved by feedback interactions that reinforce and concentrate chromatin features and factors that contribute to transcriptional silencing and exclude activating factors (Allshire and Madhani, 2018; H. Zhang et al., 2018). However, silent chromatin domains are not homogenous. Flowering plants have two major types of TE-associated silent chromatin: GC-rich coding regions of autonomous TEs, and AT-rich chromatin comprised of gene-proximal TE remnants, short non-autonomous TEs and edges of autonomous TEs (Sequeira-Mendes et al., 2014; To et al., 2020; Zemach et al., 2013; Zhong et al., 2012). Although both are comprised of TEs, these chromatin types have distinct features (Sequeira-Mendes et al., 2014; Zemach et al., 2013). How two types of silent TE chromatin are distinguished and kept separate within the nucleus is a major open question.

Both types of TE chromatin feature extensive cytosine methylation in the CG context catalyzed by MET1 (plant homolog of Dnmt1) (Cokus et al., 2008; Lister et al., 2008; Zemach et al., 2013), and are also methylated at non-CG (CHG and CHH, where H is A, T or C) cytosines (Stroud et al., 2014; Zemach et al., 2013). GC-rich TE sequences have high levels of histone modifications associated with heterochromatin, including methylation of lysine nine of histone H3 (H3K9me), and are therefore known as heterochromatic TEs (Sequeira-Mendes et al., 2014; Zemach et al., 2013). Non-CG methylation at heterochromatic TEs is catalyzed primarily by chromomethylases (CMTs; CMT3 for CHG methylation and CMT2 for CHH), which are recruited to H3K9 dimethylated (H3K9me2) nucleosomes by histone-tail-interacting domains (Du et al., 2012; Stoddard et al., 2019; Stroud et al., 2014; Zemach et al., 2013). SUVH

family H3K9me methyltransferases are in turn recruited to methylated DNA via SRA domains, forming a self-reinforcing loop (Du et al., 2014; Johnson et al., 2007; Rajakumara et al., 2011). *Arabidopsis thaliana* plants lacking functional chromomethylases (*cmt2cmt3* mutants) almost completely lack non-CG methylation at heterochromatic TEs, and their H3K9 methylation is greatly reduced (Stroud et al., 2014).

AT-rich TE sequences are low in H3K9me and other heterochromatic histone modifications, and are therefore known as euchromatic TEs (Sequeira-Mendes et al., 2014; Zemach et al., 2013). In contrast to the SUVH/CMT feedback loop that predominates in heterochromatin, RNA-directed DNA methylation (RdDM) catalyzes cytosine methylation within euchromatic TEs (Zemach et al., 2013; Zhong et al., 2012). RdDM loci are transcribed by a methylation-tolerant RNA polymerase II derivative (Pol IV) that couples co-transcriptionally with RNA-dependent RNA polymerase 2 (RDR2) to make double stranded RNA, which is processed into 23/24-nt fragments by Dicer-like 3 (DCL3). These 24-nt small RNAs (sRNA) are subsequently denatured and loaded into Argonaute (AGO) protein complexes. AGO-sRNA complexes associate with another Pol II family enzyme, Pol V, to recruit DRM DNA methyltransferases (primarily DRM2 in *Arabidopsis*) (Erdmann and Picard, 2020; Matzke and Mosher, 2014; Raju et al., 2019; Wendte and Pikaard, 2017).

Like the SUVH/CMT pathway, RdDM comprises positive feedback loops. Pol V is recruited to methylated DNA, effectively seeking its own product (Liu et al., 2014; Wongpalee et al., 2019; Zhong et al., 2012). A more paradoxical feedback loop is thought to involve recruitment of Pol IV to H3K9me (Erdmann and Picard, 2020; Matzke and Mosher, 2014; Raju et al., 2019; Wendte and Pikaard, 2017).

This hypothesis emerged from the observation that Pol IV-mediated sRNA production at many loci requires SHH1/DTF1, a protein that binds H3K9me2 and monomethylated H3K9me (H3K9me1) *in vitro* (Law et al., 2013; Zhang et al., 2013). This model of Pol IV

recruitment necessitates explaining how RdDM in general, and Pol IV specifically, is excluded from heterochromatic TEs with high H3K9me and targeted to euchromatic TEs with low H3K9me. Reliance of Pol IV on H3K9me also poses two theoretical questions. First, why would RdDM depend on a core component of the SUVH/CMT feedback loop (H3K9me2), when the two DNA methylation systems have effectively non-overlapping primary targets (Stroud et al., 2014), and RdDM targets are H3K9me-depleted? Second, the euchromatic TEs targeted by RdDM are often comprised of just one or two nucleosomes (Zemach et al., 2013). Maintenance of histone modifications is expected to be unstable at such short sequences due to the random partitioning of nucleosomes to sister chromatids following DNA replication (Angel et al., 2011; Berry and Dean, 2015; Lövkvist and Howard, 2021; Ramachandran and Henikoff, 2015; Zilberman and Henikoff, 2004). Why would RdDM, a pathway capable of almost nucleotide-level resolution (Blevins et al., 2015; Zhai et al., 2015) and specialized for silencing short TEs, be tied to a histone modification that requires longer sequences for stable propagation?

Here, we show that Pol IV activity is recruited to sequences with non-CG DNA methylation regardless of H3K9me, so that both the Pol IV and Pol V branches form positive feedback loops with the ultimate product of RdDM. We also show that linker histone H1 impedes RdDM activity in GC-rich heterochromatin, thereby restricting RdDM to AT-rich euchromatic TE. We propose that without H1, RdDM would be diluted into and effectively incapacitated by the vast stretches of non-CG methylated heterochromatin common in plant genomes (Feng et al., 2010; Niederhuth et al., 2016; Ritter and Niederhuth, 2021; Zemach et al., 2010). The affinity of H1 for GC-rich heterochromatin (Choi et al., 2020) focuses RdDM activity on short, AT-rich euchromatic TEs that RdDM is uniquely suited to silence.

Results

Histone H1 levels predict the global bifurcation of non-CG DNA methylating systems

To understand how the CMT and RdDM pathways are separated, we categorized *Arabidopsis* TEs by the dependence of their CHH methylation (mCHH) either on CMT2 (CMT TEs) or DRM2 (DRM TEs). Among 18785 TEs with more than 2% mCHH in wild type (*wt*) plants, 4486 TEs were demethylated in *cmt2* plants and 3039 TEs lost mCHH in *drm2* (mCHH in the mutants <0.02, Fisher's exact test p <0.01, TEs longer than 200 bp; Figure S1A and Table S1). Only 80 TEs lost mCHH methylation in both mutants (Table S1), consistent with the largely separate sets of DRM and CMT targets (Sigman and Slotkin, 2016; Stroud et al., 2014). Next, we used random forest classification (Breiman, 2001; Ishwaran et al., 2010) to identify predictors of DRM or CMT targets (Figure 1A). We included genetic and epigenetic features known to be associated with RdDM or CMT activity, as well as linker histone H1. H1 is specifically enriched in heterochromatic TEs, and its loss leads to increased DNA methylation at heterochromatic TEs and decreased methylation at euchromatic ones (Bourguet et al., 2021; Lyons and Zilberman, 2017; Papareddy et al., 2020; Rutowicz et al., 2015; Zemach et al., 2013). As expected, sRNA abundance can distinguish CMT and DRM TEs (Figure 1A). H3K9me1 is also a good classifier (Figure 1A). However, the best classifier turned out to be H1 (Figure 1A). Using all variables in Figure 1A, we could predict CMT and DRM TEs with an error rate of 2.15% (Figure 1B). With just H3K9me1 and H1, the prediction is almost as accurate (5.42% error; Figure 1B). Remarkably, H1 alone successfully identifies CMT and DRM TEs (12.17% error; Figure 1B), suggesting that H1 is fundamental to separating these silencing pathways.

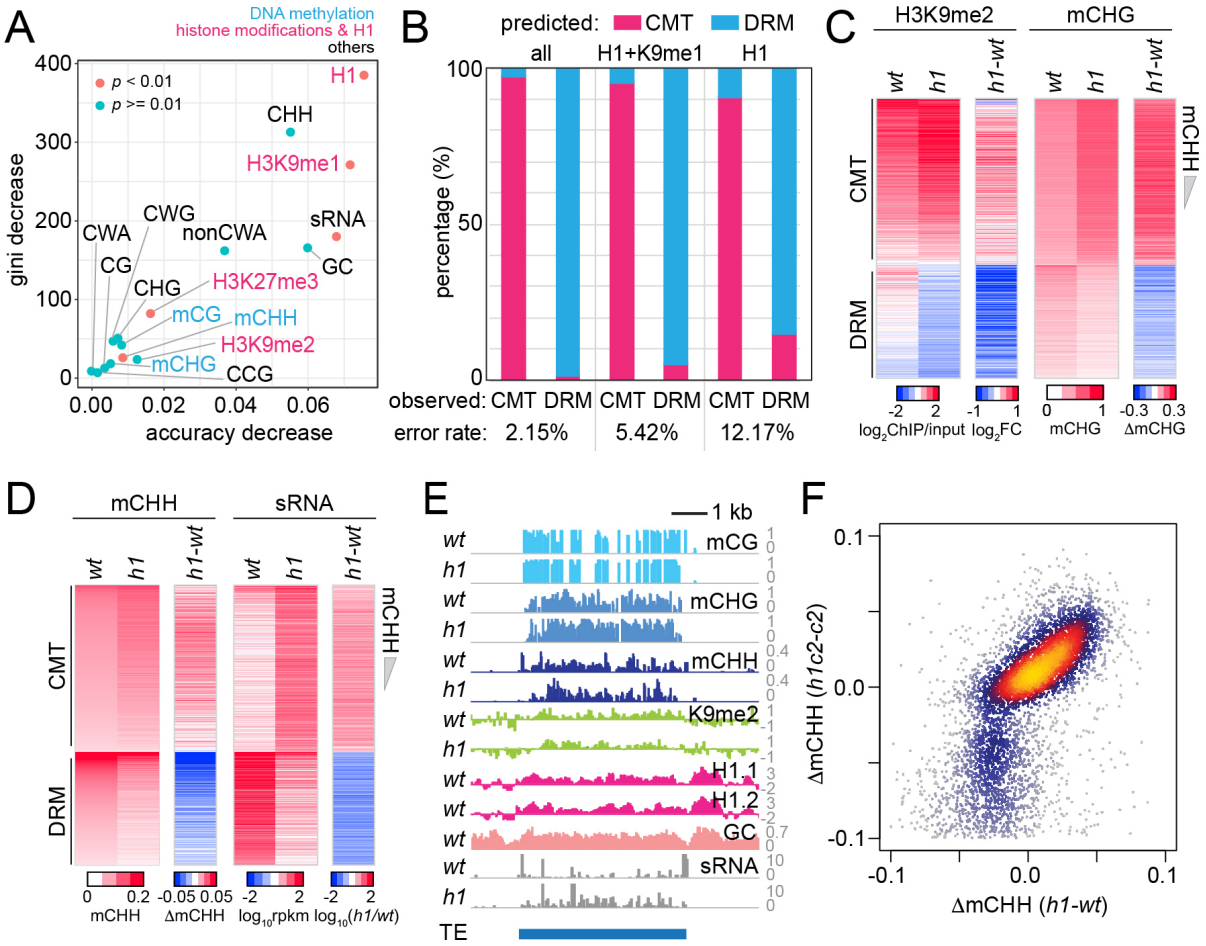

115 **Figure 1** Histone H1 prohibits RNA-directed DNA methylation of CMT-dependent
116 heterochromatic transposons.

117 **(A)** The importance of DNA methylation, histone H3 modifications, sRNA, H1, and cytosine
118 sequence context to predict CMT TE or DRM TE classes by random forest classification. **(B)**
119 Prediction of CMT or DRM TE classes by random forest classification with all variables, H1
120 and H3K9me1, or only H1. **(C** and **D)** Heatmaps of H3K9me2 and mCHG levels **(C)** and
121 mCHH and sRNA levels **(D)** at CMT and DRM TEs in *wt* and *h1* plants. TEs were sorted by
122 mCHH level in *wt*. **(E)** Example of DNA methylation and sRNA expression at a CMT TE in
123 *wt* and *h1* (AT1TE58075). **(F)** mCHH difference between *wt* and *h1* (x-axis) versus *h1cmt2*
124 (*h1c2*) and *cmt2* (*c2*; y-axis) at CMT TEs.

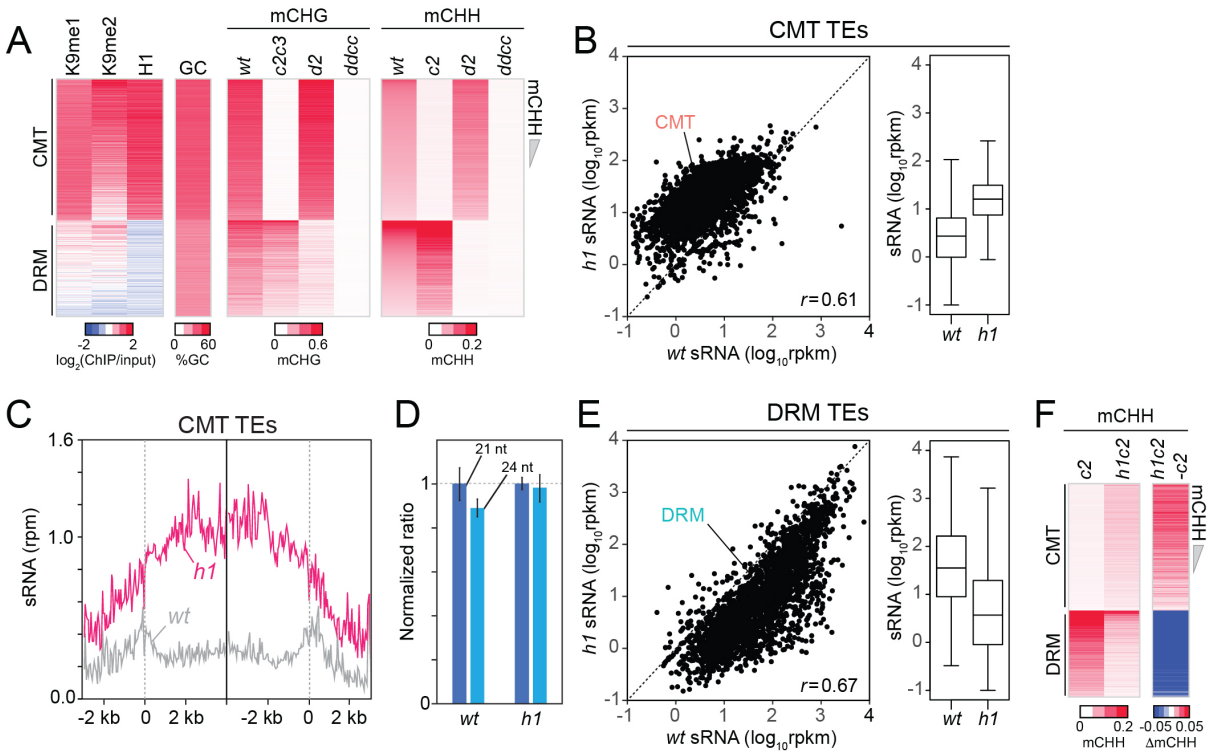

125 **Figure S1** CMT TEs gain non-CG DNA methylation and sRNA expression in *h1* plants.
126 **(A)** Heatmaps of H3K9me, H1, GC content, mCHG, and mCHH at CMT and DRM TEs in *wt,*
127 *cmt2* (*c2*), *cmt2cmt3* (*c2c3*), *drm2* (*d2*), and *drm1drm2cmt2cmt3* (*ddcc*) plants. TEs were sorted
128 by mCHH level in *wt*. **(B)** Average sRNA expression level of CMT TEs in *wt* and *h1* plants.
129 **(C)** Average sRNA distribution around CMT TEs in *wt* and *h1* plants. **(D)** Normalized number
130 of mapped reads of 21-nt and 24-nt length sRNAs in *wt* and *h1* plants. The number of mapped
131 reads of 21-nt sRNA was normalized to 1. **(E)** Average sRNA expression level of DRM TEs
132 in *wt* and *h1* plants. **(F)** Heatmaps of mCHH in *c2* and *h1cmt2* (*h1c2*) plants. TEs were sorted
133 by mCHH level in *wt.* **(B** and **E)** rpkm indicates reads per kilobase of transcript, per million
134 mapped reads. *r* indicates Pearson's correlation. **(C)** rpm indicates reads per million mapped
135 reads.

RdDM activity relocates to heterochromatin without H1

To understand how H1 regulates the CMT and DRM pathways, we analyzed 24-nt sRNA expression, DNA methylation, and H3K9me2 in *h1* plants that have inactivating mutations in both of the canonical *Arabidopsis* H1 genes (Zemach et al., 2013). Consistent with published results (Bourguet et al., 2021; Lyons and Zilberman, 2017; Papareddy et al., 2020; Rutowicz et al., 2015; Zemach et al., 2013), we found an elevation of CHG methylation (mCHG), H3K9me2 and mCHH at CMT TEs (Figure 1C-D). CMT TEs are depleted of sRNAs in *wt*, but sRNA expression increases 5.6-fold in *h1* plants (Figure 1D, Figure S1B and S1C). sRNA expression in *h1* positively correlates with that in *wt* (Figure S1B), indicating that loss of H1 amplifies sRNA expression at RdDM-capable CMT TEs rather than creating *de novo* RdDM targets.

In contrast to the hypermethylation of CMT TEs, DRM TEs lose H3K9me2, mCHG, mCHH and sRNA expression in *h1* plants (Figure 1C-D and Figure S1E). Despite the loss of sRNA at DRM TEs, global 24-nt sRNA abundance is not altered in *h1* plants (Figure S1D), indicating the reallocation of RdDM activity from DRM to CMT TEs. This phenomenon can be observed within individual TEs, with sRNA biogenesis and mCHH relocating from the AT-rich edges in *wt* to the GC-rich internal sequences in *h1* (Figure 1E). CMT TE mCHH increases to the same relative extent in *h1* plants devoid of CMT2 (*h1c2*; Figure 1F and Figure S1F), indicating that mCHH hypermethylation at CMT TEs in *h1* mutants is caused by RdDM. These results indicate that RdDM relocates into heterochromatin in the absence of H1 and are consistent with recently published work (Bourguet et al., 2021; Papareddy et al., 2020).

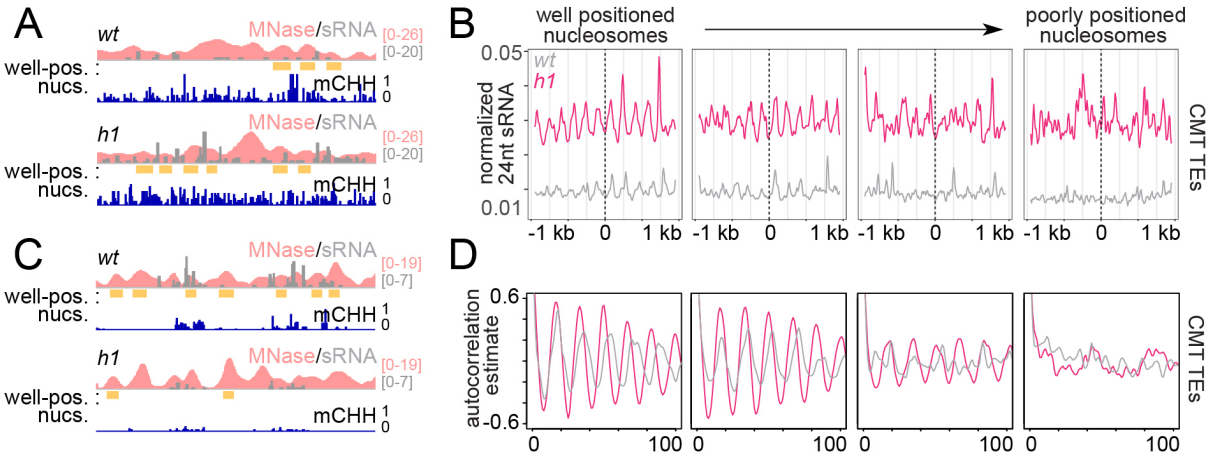

157 **Figure 2** RdDM is preferentially active in linker DNA in *h1* plants.

158 **(A** and **C)** Example of a CMT TE (Chr2:3,944,600-3,946,400) (**A**) and DRM TE

159 (Chr2:6,389,500-6,392,500) (**C**) with well-positioned nucleosomes (yellow boxes). Smoothed

160 MNase-seq (apricot), sRNA expression (gray) and mCHH (indigo) are plotted. **(B)** Average

161 sRNA expression around well positioned or poorly positioned nucleosomes at CMT TEs. **(D)**

162 Autocorrelation estimates of average sRNA values shown in (**B**) to illustrate shortened sRNA

163 phasing in *h1* mutants corresponding to shortened nucleosome repeat length.

164 **Lack of H1 promotes sRNA biogenesis in linker DNA**

165 Absence of H1 in *Arabidopsis* causes a preferential increase of heterochromatic TE DNA

166 methylation within linker DNA, the regions between nucleosomes (Lyons and Zilberman,

167 2017). The average distance between heterochromatic nucleosomes is also reduced from ~180

168 to 167 bp (Choi et al., 2020). Given the relative promiscuity of RNA Pol IV initiation (Zhai et

169 al., 2015) and the increased sRNA abundance at CMT TEs in *h1* (Figure 1D, Figure S1B and

170 S1C), we asked whether patterns of sRNA production with respect to nucleosomes are altered

171 in *h1*. As expected, overall levels of sRNA are increased around nucleosomes of CMT TEs and

172 decreased at DRM TEs (Figure 2A-C and Figure S2). An overt sRNA linker bias is apparent

173 in both *h1* and *wt* around the best-positioned nucleosomes (Figure 2A-C and Figure S2). This

174 pattern becomes less obvious at less-well-positioned loci until it disappears completely (Figure

2B and Figure S2), as illustrated by measuring the correlation of the sRNA signal to itself (Figure 2D). The shortening *h1* sRNA autocorrelation around better positioned nucleosomes (Figure 2D) demonstrates how the linker histone dictates sites of sRNA production directly through linker occlusion and indirectly through nucleosome positioning.

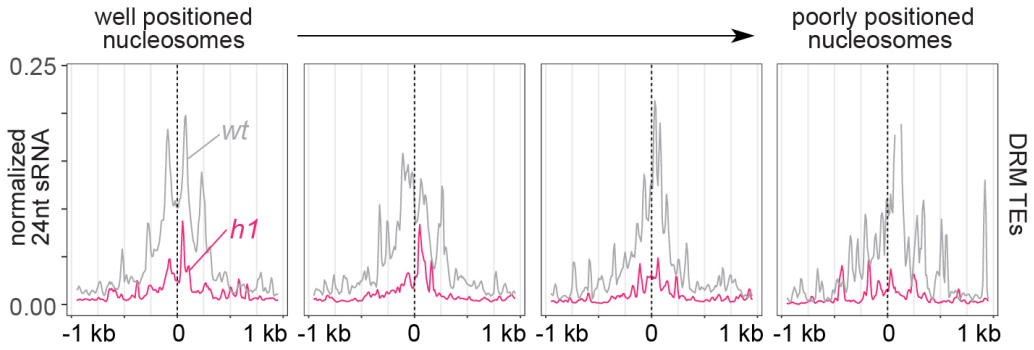

Figure S2 RdDM is enriched at linker DNA around well positioned nucleosomes. Average sRNA expression around well positioned (left) to increasingly poorly positioned nucleosomes at DRM TEs.

RdDM is recruited to CMT TEs independently of SHH1

Because H3K9me is thought to recruit Pol IV activity (Law et al., 2013; Zhang et al., 2013), we investigated how sRNA distribution changes in relation to H3K9me1/2 in *h1* plants. In *wt*, sRNA expression increases as H3K9me1 and H3K9me2 levels rise, but this trend reverses at TEs with more H3K9me and H1 (Figure 3A and 3B). In contrast, sRNA expression shows a relatively simple, direct relationship with H3K9me1 and H3K9me2 in *h1* plants (Figure 3A and 3B), suggesting that H1 prevents Pol IV from following the H3K9me gradient.

The only H3K9me binding factor implicated in Pol IV recruitment is SHH1 (Law et al., 2013; Zhang et al., 2013; Zhou et al., 2018). Therefore, we tested whether CMT TE hypermethylation in *h1* plants requires SHH1. CMT TEs remain hypermethylated in

192 *h1cmt2shh1* plants to about the same extent as in *h1cmt2* plants (Figure 3C), demonstrating
193 that in the absence of H1, Pol IV is recruited to CMT TEs independently of SHH1.

194 Pol IV activity depends on a family of four CLSY putative chromatin remodeling
195 proteins (Greenberg et al., 2013; Smith et al., 2007; Zhou et al., 2018). Simultaneous loss of
196 CLSY1 and CLSY2 has the same effect as loss of SHH1, whereas CLSY3 and CLSY4 mediate
197 RdDM at a largely distinct set of loci (Yang et al., 2018; Zhou et al., 2018). Mutations of SHH1
198 and CLSY1/2 preferentially reduce mCHH and sRNA at DRM TEs and increase mCHH at
199 CMT TEs (Figure 3C). In contrast, *clsy3/4* mutant plants have reduced mCHH and sRNA at
200 CMT TEs and increased mCHH and sRNA at DRM TEs (Figure 3C), suggesting that SHH1
201 and CLSY1/2 preferentially mediate RdDM at DRM TEs, whereas CLSY3/4 preferentially
202 recruit Pol IV to CMT TEs. Consistently, TEs hypermethylated in *h1cmt2* and *h1cmt2shh1*
203 show a strong overlap with published CLSY3/4-dependent sRNA clusters and little overlap
204 with CLSY1/2-dependent clusters (Figure 3D and Figure S3). Overall, our results indicate that
205 SHH1 is relatively unimportant for RdDM activity at H3K9me-rich CMT TEs with or without
206 H1. The entry of Pol IV into H1-depleted heterochromatin must either involve a different
207 H3K9me interacting factor, or a chromatin feature other than H3K9me.

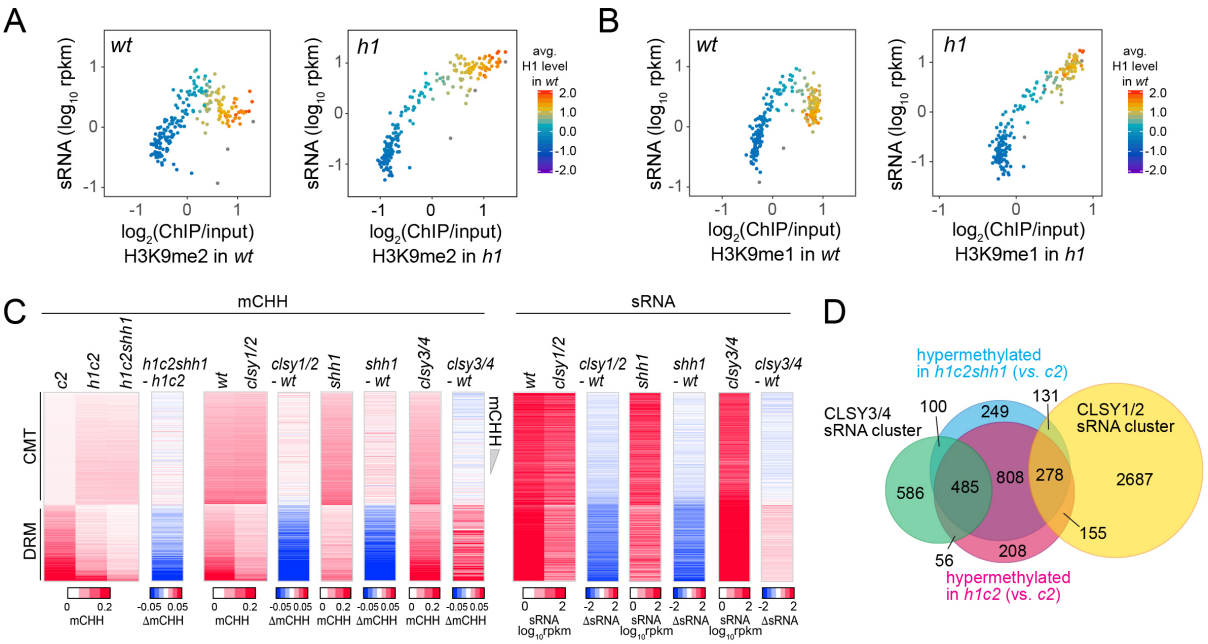

208 **Figure 3** SHH1 is not required for non-CG hypermethylation in *h1*.

209 **(A** and **B)** Average H3K9me2 **(A)** or H3K9me1 **(B)** (x-axis) and sRNA expression level (y-

210 axis) in *wt* and *h1*. Each dot represents the average of 100 TEs sorted by GC content. **(C)**

211 Heatmaps of mCHH and sRNA expression at CMT and DRM TEs in plants with *shh1* or *clsy*

212 mutations. **(D)** Venn diagram of TEs in indicated categories.

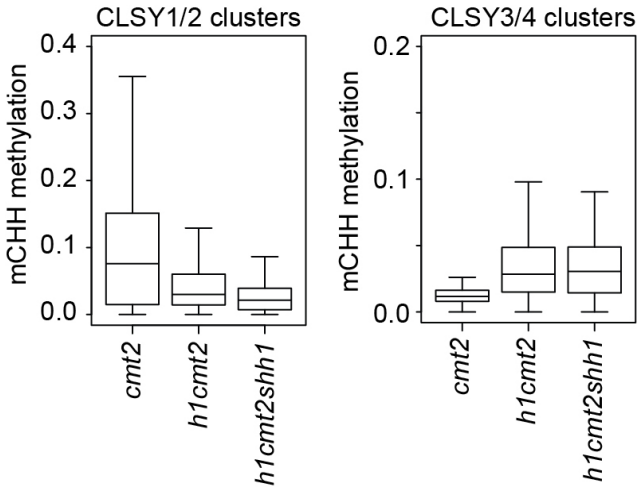

213 **Figure S3** Loss of *h1* causes CMT2-independent hypermethylation at TEs with CLSY3/4

214 sRNA clusters. Boxplots show mCHH at TEs within indicated CLSY clusters.

RdDM expansion does not require CG methylation

Our results suggest that sRNA biogenesis at CMT TEs in *h1* mutants is mediated by CLSY3/4 Pol IV complexes. Recruitment of these complexes has been proposed to involve CG methylation (mCG) (Zhou et al., 2018). Therefore, we examined sRNA levels and DNA methylation in *h1met1* mutants (Choi et al., 2020). Although MET1 is a CG methyltransferase, its loss also perturbs non-CG methylation and H3K9me2 at some CMT TEs (Figure 4A and Figure S4A) (Choi et al., 2020; Deleris et al., 2012; Yaari et al., 2015; Zabet et al., 2017; Y. Zhang et al., 2018). To understand how these changes impact sRNA production, we differentiate between two groups of CMT TEs in *met1* plants. MET1-independent CMT TEs keep non-CG methylation and H3K9me2 in *met1* (Figure S4A) (Choi et al., 2020) and accordingly maintain sRNA expression (Figure 4B). These CMT TEs gain sRNA expression and mCHH in *h1met1* relative to *met1* and *wt* (Figure 4B), demonstrating that mCG is not required for RdDM expansion into heterochromatin caused by H1 loss. In contrast, MET1-dependent CMT TEs, which lose non-CG methylation and H3K9me in *met1* (Figure S4A) (Choi et al., 2020), lose sRNA in *met1* and do not recover sRNA expression or mCHH in *h1met1* (Figure 4C), suggesting that non-CG methylation or H3K9me is necessary for sRNA biogenesis.

To test the above hypothesis, we grouped CLSY3/4 targets by mCHH level in *met1* (mCHH≥0.05 in *wt* and *met1*; mCHH≥0.05 in *wt* and <0.05 in *met1*). Even though all CLSY3/4 targets lose mCG in *met1*, sRNA expression is reduced only when non-CG methylation and H3K9me2 are reduced (Figure 4D and Figure S4B), implying that the presence of non-CG methylation and/or H3K9me is sufficient to maintain CLSY3/4-dependent sRNA biogenesis. In *h1met1*, sRNA levels increase at CLSY3/4 targets where non-CG methylation is maintained: among 1565 CLSY3/4 clusters with *wt* non-CG methylation (>0.01%), 72% keep non-CG methylation in *met1* and gain sRNA expression in *h1met1*, whereas 28% lose non-CG

methylation in *met1* and have similarly low sRNA levels in *met1* and *h1met1* (Figure 4E and Figure S4C). These results indicate that neither CLSY3/4 Pol IV activity, nor the RdDM expansion triggered by loss of H1, depend on mCG.

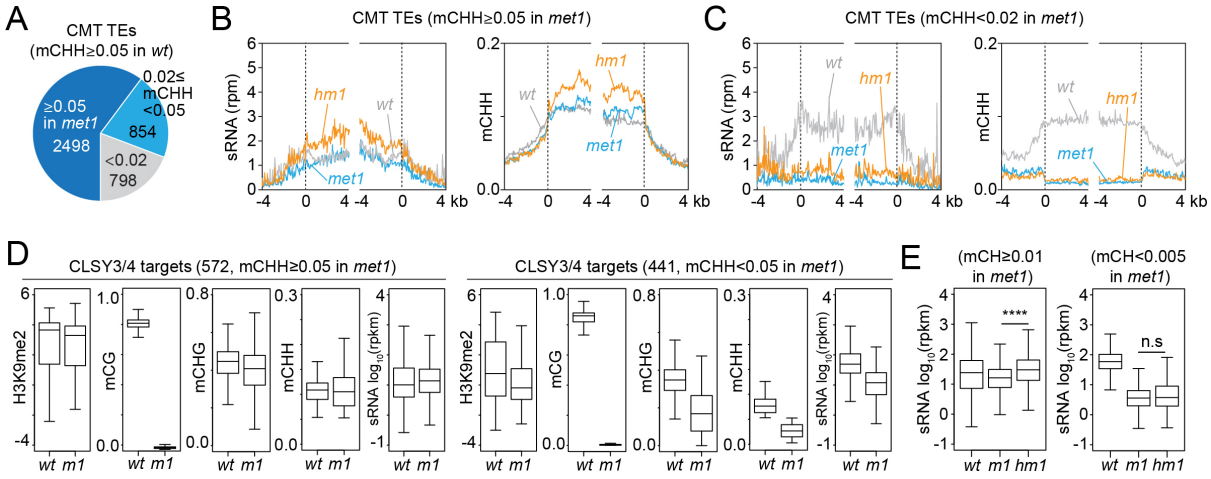

Figure 4 sRNA expression at CLSY3/4 clusters is independent of mCG.

(A) The number of CMT TEs (mCHH≥0.05 in *wt*) that maintain mCHH in *met1* (mCHH≥0.05 in *met1*; 2498) or lose mCHH in *met1* (mCHH<0.02 in *met1*; 798). **(B** and **C)** Averaged sRNA distribution and mCHH levels around CMT TEs in *wt*, *met1*, and *h1met1* (*hm1*) plants that maintain mCHH in *met1* (mCHH≥0.05 in *met1*; **B**) and lose mCHH in *met1* (mCHH<0.02 in *met1*; C). **(D)** Boxplots of H3K9me2, DNA methylation, and sRNA expression at CLSY3/4 sRNA clusters in *wt* and *met1* (*m1*). CLSY3/4 clusters that maintain more than 5% mCHH in *met1* or less than 5% mCHH in *met1* are plotted separately. **(E)** sRNA expression level at CLSY3/4 sRNA clusters that maintain non-CG methylation (mCH≥0.01) in *met1* or lose non-CG methylation (mCH<0.005) in *met1*. Non-CG methylation (mCH) density equals number of mCH sites per base pair.

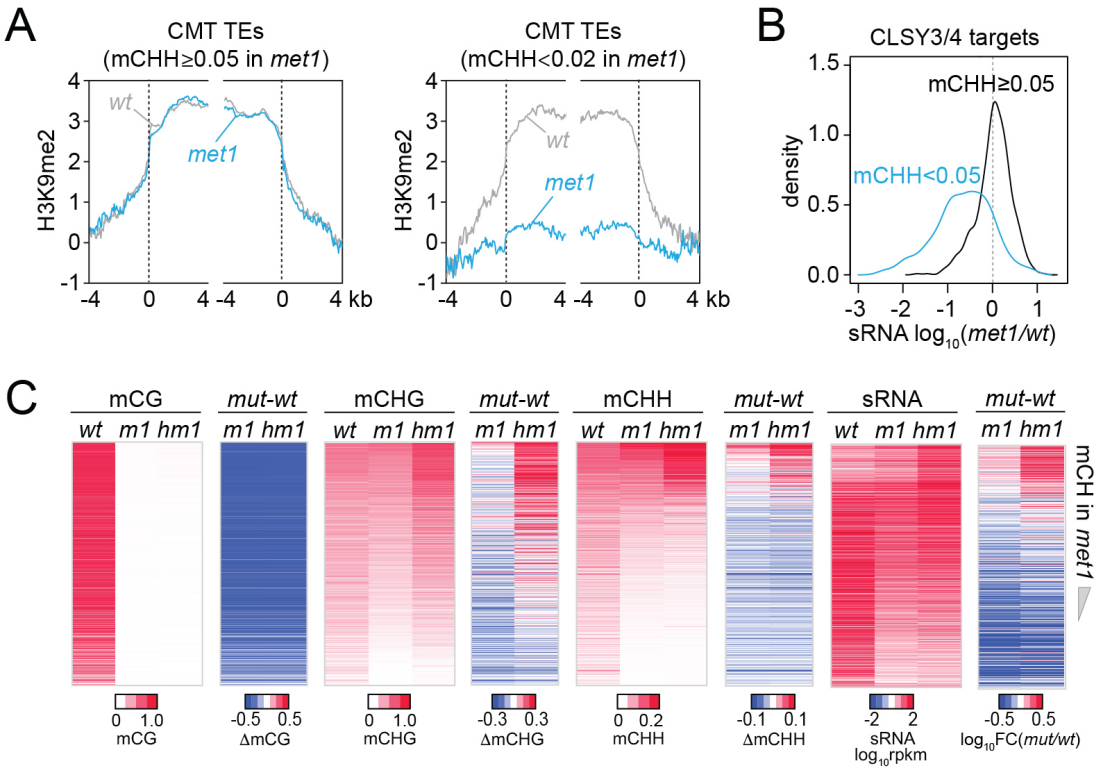

Figure S4 DNA methylation and sRNA expression changes in *met1* and *h1met1*.

(A) H3K9me2 levels around CMT TEs that maintain mCHH (mCHH≥0.05) in *met1* and lose mCHH (mCHH<0.02) in *met1*. **(B)** Kernel density distribution of sRNA expression changes at CLSY3/4 sRNA clusters in *met1* (vs. *wt*) that maintain more than 5% mCHH in *met1* or less than 5% mCHH in *met1*. **(C)** Heatmaps of DNA methylation and sRNA expression at CMT TEs in *wt*, *met1* (*m1*), and *h1met1* (*hm1*). TEs were sorted by non-CG methylation level (mCH) in *met1*.

Severe H3K9me reduction does not perturb RdDM expansion into heterochromatin

Our results so far indicate that H1 prevents RdDM from following a gradient of either H3K9me or non-CG methylation into heterochromatin. However, heterochromatin is structurally complex and contains many factors (Feng and Michaels, 2015). To understand the overall importance of heterochromatin integrity, we tested the effects of H1 on sRNA distribution in plants with a mutation in the Swi/Snf2 chromatin remodeler DDM1, which have severely

compromised heterochromatin (Kim and Zilberman, 2014; Sigman and Slotkin, 2016). The *ddm1* mutation greatly reduces heterochromatic DNA and H3K9 methylation (Ito et al., 2015; Lyons and Zilberman, 2017; Osakabe et al., 2021; Teixeira et al., 2009; Zemach et al., 2013), activates TE expression (Lippman et al., 2004; Osakabe et al., 2021; Panda et al., 2016; Panda and Slotkin, 2020; Rougée et al., 2020) and disperses nuclear heterochromatic foci (Rougée et al., 2020; Soppe et al., 2002) (Figure 5A-B and Figure S5A). However, 24-nt sRNA expression in *ddm1* is broadly similar to *wt* (Figure 5C-D and Figure S5B). Simultaneous lack of H1 and DDM1 in *h1ddm1* mutants (Lyons and Zilberman, 2017; Zemach et al., 2013) causes relocation of sRNA biogenesis into CMT TEs that mirrors that in *h1* plants (Figure 5C and Figure S5B), indicating that overall heterochromatin integrity is not required for this process. Furthermore, RdDM expansion into heterochromatin occurs in *h1ddm1* despite strong H3K9me reduction compared to *wt* and *h1* (Figure 5A-B and Figure S5A). This does not rule out the possibility that H3K9me promotes Pol IV activity, because the H3K9me remaining in *h1ddm1* may be sufficient. However, the observation that sRNA production at CMT TEs is largely unaffected by a bulk H3K9me reduction argues against a primary role for H3K9me in Pol IV recruitment.

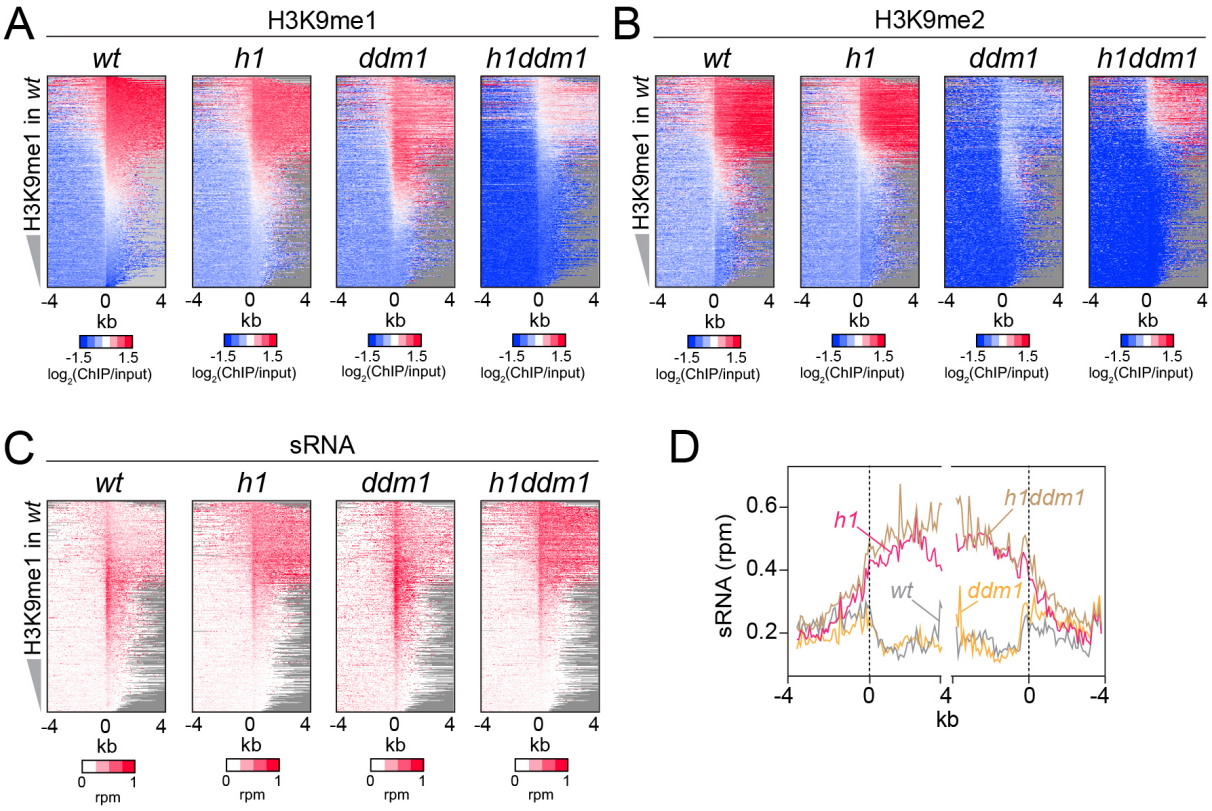

282 **Figure 5** Severely reduced H3K9 methylation does not prevent sRNA expansion.

283 **(A-C)** Distribution of H3K9 methylation (**A** and **B**) and sRNA expression (**C**) around 5' ends

284 of TEs in *wt*, *h1*, *ddm1*, and *h1ddm1* plants. **(D)** Averaged sRNA distribution around CMT TEs

285 in *wt*, *h1*, *ddm1*, and *h1ddm1* plants.

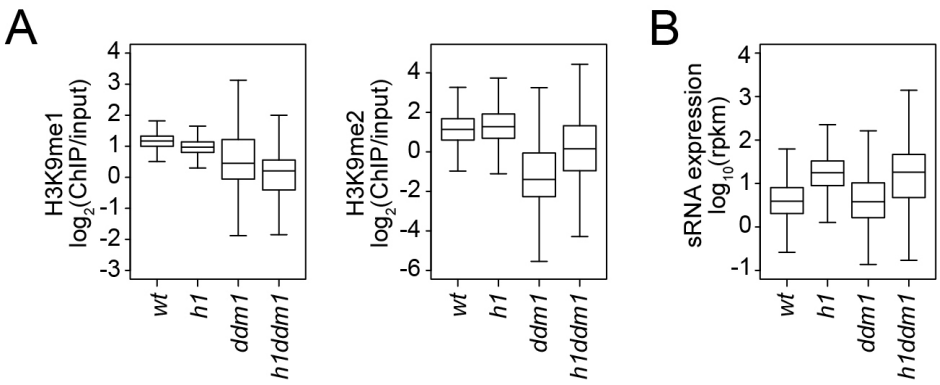

286 **Figure S5** sRNA expression and H3K9 methylation changes in *h1, ddm1* and *h1ddm1*.
287 **(A** and **B)** Boxplots of H3K9 methylation levels **(A)** and sRNA expression **(B)** at CMT TEs in
288 *wt, h1, ddm1,* and *h1ddm1* plants.

289 **H3K9me and non-CG methylation can be decoupled in heterochromatin**

290 H3K9me and non-CG DNA methylation are closely associated in heterochromatin due to the
291 feedback loop between CMT2/3 and the SUVH4/5/6 H3K9 methyltransferases (Du et al., 2012;
292 Stoddard et al., 2019; Stroud et al., 2014). To isolate the effects of these features on sRNA
293 biogenesis, we examined DNA methylation, H3K9me and sRNA levels in *c2c3* and *h1c2c3*
294 plants. While CG methylation is largely unaffected, non-CG methylation is specifically
295 abolished at CMT TEs in these plants (Figure S6A), consistent with previously published *c2c3*
296 results (Stroud et al., 2014). As expected, H3K9me is also greatly reduced (Figure S6A), but
297 some H3K9me1 and H3K9me2 remains in heterochromatin. Specifically, 875 CMT TEs
298 maintain H3K9me1 and 1126 maintain H3K9me2 in *c2c3*, while in *h1c2c3* we identified 2434
299 H3K9me1-enriched CMT TEs and 1443 H3K9me2-enriched CMT TEs (Figure 6A and 6B).
300 Principal component analysis shows that H3K9me in these mutants associates with mCG,
301 followed by CG and CCG density (which contributes to mCG density; Figure 6C and S6B),
302 suggesting that SUVH4/5/6 are recruited to mCG in the absence of non-CG methylation.

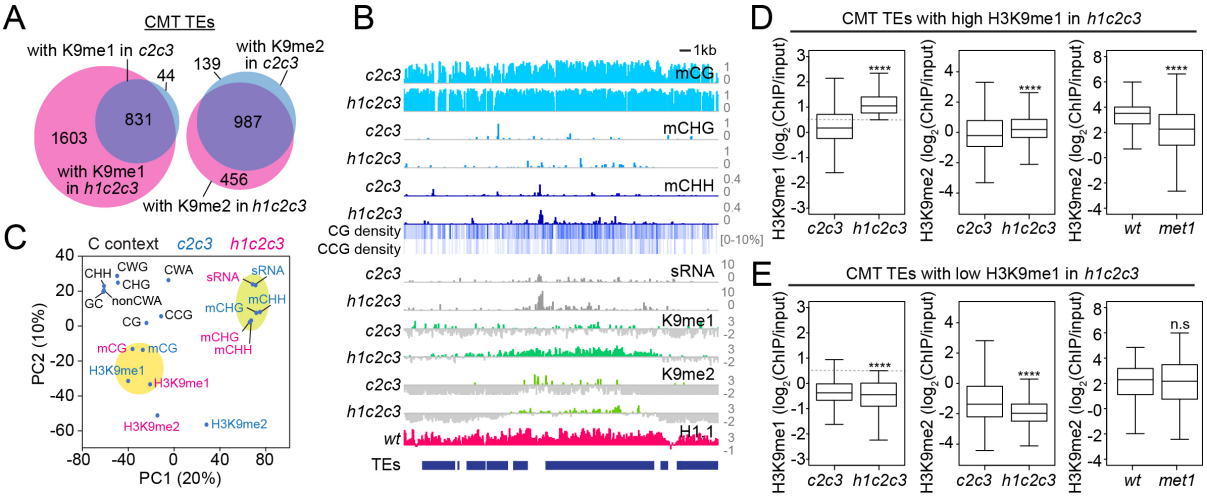

Figure 6 Non-CG DNA methylation and H3K9 methylation are decoupled in *h1c2c3*. **(A)** Number of CMT TEs with H3K9 methylation (average H3K9me1 (K9me1) or H3K9me2 (K9me2) > 0.5) in *cmt2cmt3* (*c2c3*) or *h1cmt2cmt3* (*h1c2c3*) plants. **(B)** Example of DNA methylation, CG and CCG density, H1 level, H3K9 methylation and sRNA expression around CMT TEs in *c2c3* and *h1c2c3* plants (Chr3:14,495,000-14,520,000). **(C)** Principal component analysis of H3K9me, cytosine content (total GC content, CG, CCG, CHG, CHH, CWG, CWA, and nonCWA (W=A and T)), DNA methylation, and sRNA expression in *c2c3* and *h1c2c3* plants. **(D** and **E)** H3K9me levels at CMT TEs with high H3K9me1 (H3K9me1 ≥ 0.5; **D**) or low H3K9me1 (H3K9me1 < 0.5; **E**) in *h1c2c3* plants.

This conclusion is supported by a complementary pattern of H3K9 methylation changes in *h1c2c3* vs. *met1*. TEs that lose H3K9me2 in *met1,* suggesting H3K9me dependence on mCG, maintain H3K9me in the absence of mCHG/mCHH in *h1c2c3* (Figure 6D). Conversely, TEs that lose H3K9me in *h1c2c3,* suggesting H3K9me dependence on mCHG/mCHH, retain H3K9me2 in *met1* (Figure 6E). This indicates that H3K9me at mCG-dense CMT TEs is partially dependent on mCG, leading to considerable H3K9me retention in *c2c3*, and especially *h1c2c3* plants. The ability of mCG to recruit H3K9me is consistent with published work, including studies that show RdDM-independent initiation of the CMT-SUVH feedback loop

specifically at CG-methylated sequences (Miura et al., 2009; To et al., 2020; Zabet et al., 2017) and the observed affinity of SUVH histone methyltransferase SRA domains for mCG *in vitro* (Johnson et al., 2007; Li et al., 2018; Rajakumara et al., 2011).

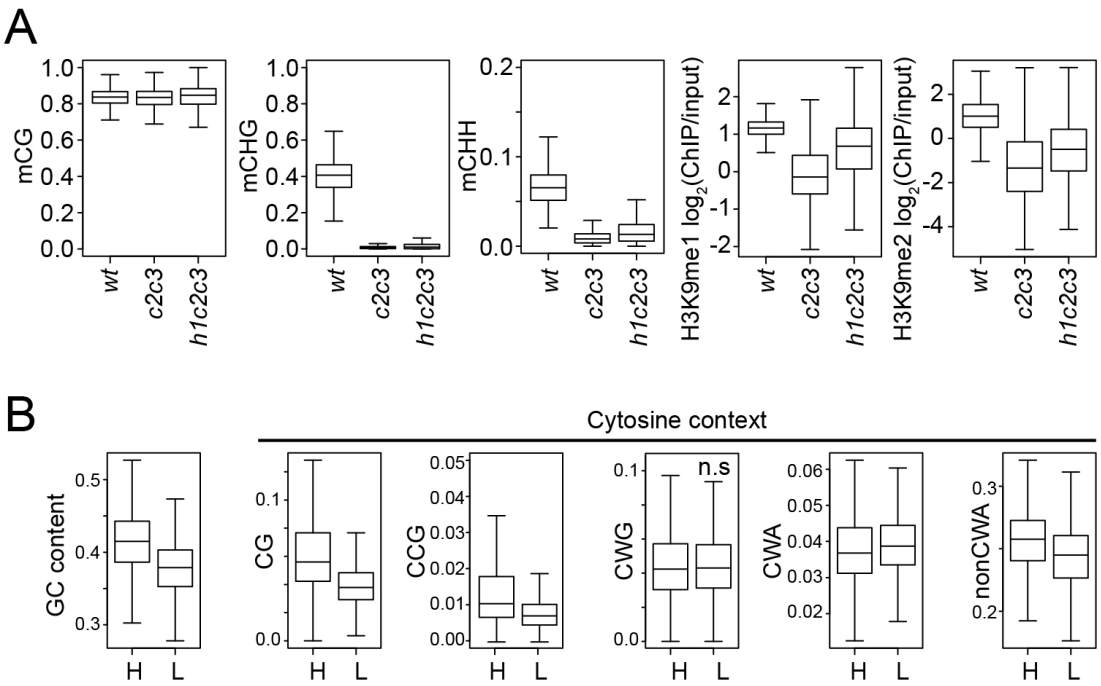

Figure S6 Analysis of chromatin features at CMT TEs.

(A) Boxplots of DNA methylation and H3K9 methylation levels at CMT TEs in *wt, cmt2cmt3* (*c2c3*), and *h1cmt2cmt3* (*h1c2c3*) plants. **(B)** Cytosine context density (total GC content, CG, CCG, CWG, CWA, and nonCWA (W=A and T)) at CMT TEs with high H3K9me1 (H3K9me1 ≥ 0.5; H) and low H3K9me1(H3K9me1 < 0.5; L) in *h1c2c3* plants.

24-nt sRNA production specifically correlates with non-CG methylation

The decoupling of H3K9me and non-CG methylation in *h1c2c3* plants allowed us to determine how each feature is associated with sRNA biogenesis. In *h1* plants, H3K9me2, DNA methylation in every context, and sRNA expression together increase in direct relation to *wt* H1 prevalence, as loss of H1 increases accessibility of previously H1-rich TEs (Figure 7A and Figure S7A) (Bourguet et al., 2021; Lyons and Zilberman, 2017; Papareddy et al., 2020;

Zemach et al., 2013). H3K9me1/2, DNA methylation, and sRNA levels are also all positively correlated in *h1* plants, though the correlation between H3K9me2 and sRNA is weak (Figure 7B and Figure S7B). In contrast, the coupling of H3K9me with DNA methylation and sRNA levels nearly disappears when comparing *h1c2c3* to *c2c3* (Figure 7C-D and Figure S7C-D). Relative H3K9me1/2 abundance increases with *wt* H1 levels, whereas DNA methylation and sRNA changes show at best a very weak relationship with *wt* H1 enrichment (Figure 7C and Figure S7C). Two correlated groups remain in *h1c2c3*: H3K9me1/2 with mCG, and sRNA with mCHG/mCHH (Figure 7D and Figure S7D). The linear correlations between sRNA and either H3K9me1 or mCG observed in *h1* (Figure 7E) become kinked in *h1c2c3* (Figure 7F). Only the association between non-CG methylation and sRNA remains linear (Figure 7E and 7F). This dynamic can be observed at an individual array of CMT TEs (Figure 7G). 24-nt sRNA expression is confined to the edges of the CMT TE array in *wt*, but follows H3K9me and DNA methylation throughout the array in *h1* plants (Figure 7G). In *h1c2c3*, non-CG methylation within the array is strongly reduced, but H3K9me is maintained, and sRNA expression is associated with remaining mCHH but not with H3K9me (Figure 7G). Altogether, these results do not support the hypothesis that Pol IV is recruited by H3K9me, and offer non-CG methylation as the most likely alternative.

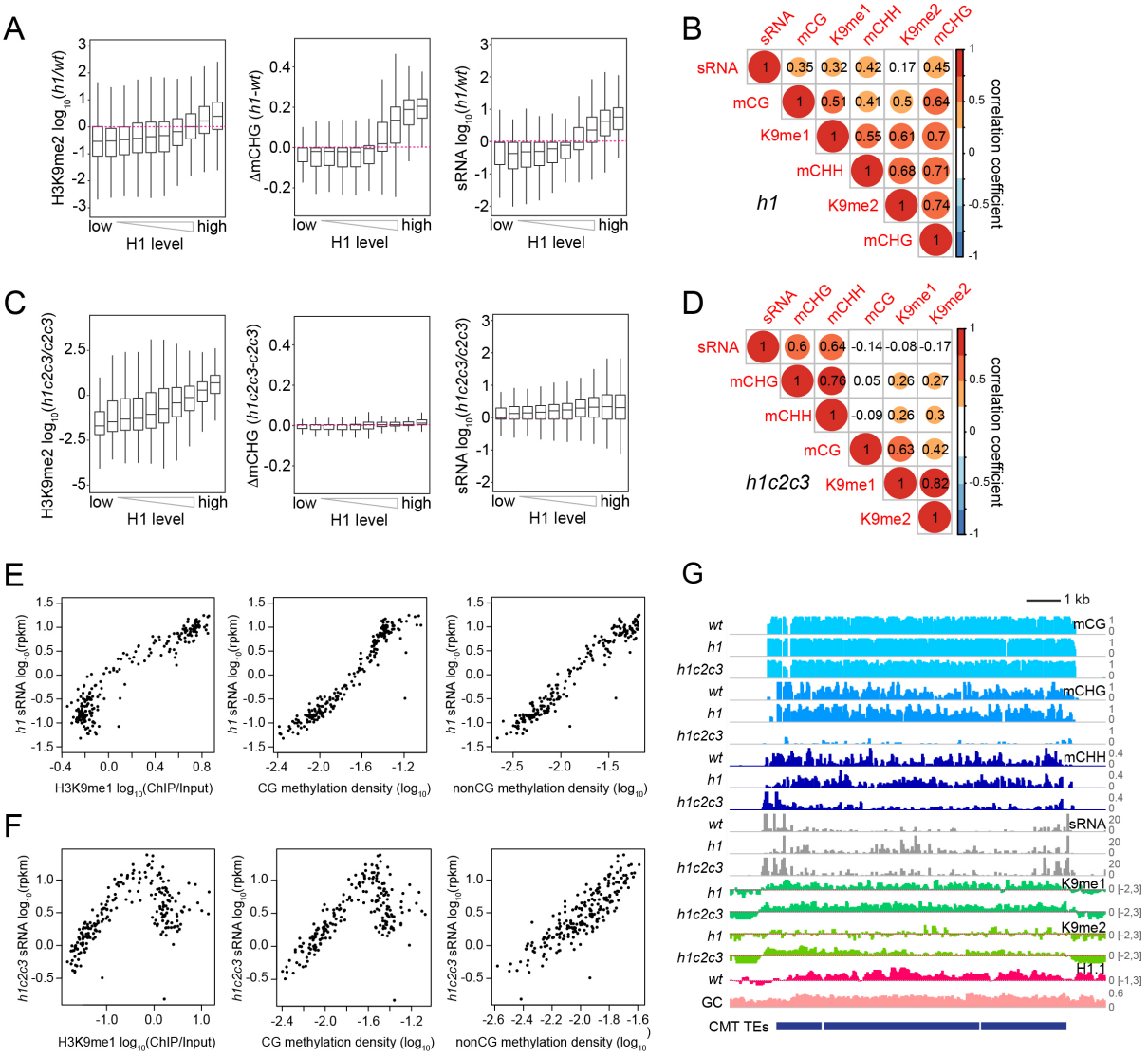

Figure 7 sRNA expression specifically correlates with non-CG methylation.

(A and **C)** Boxplots of H3K9me2, mCHG, and sRNA expression changes in *h1* vs. *wt* (**A**) and *h1c2c3* vs. *c2c3* (**C**). **(B** and **D)** Correlation among H3K9 methylation, DNA methylation, and sRNA expression in *h1* plants (**B**) and *h1c2c3* plants (**D**). **(E** and **F)** sRNA expression relation to H3K9me1, CG and non-CG methylation density in *h1* plants (**E**) and *h1c2c3* plants (**F**). Each dot represents the average of 100 TEs sorted by GC content. DNA methylation density equals number of methylated sites per base pair. **(G)** Example of DNA methylation, sRNA expression, H3K9 methylation (K9me1 and K9me2), and H1.1 distribution at CMT TEs in *wt, h1,* and *h1c2c3* plants (Chr2:6,548,000-6,559,000).

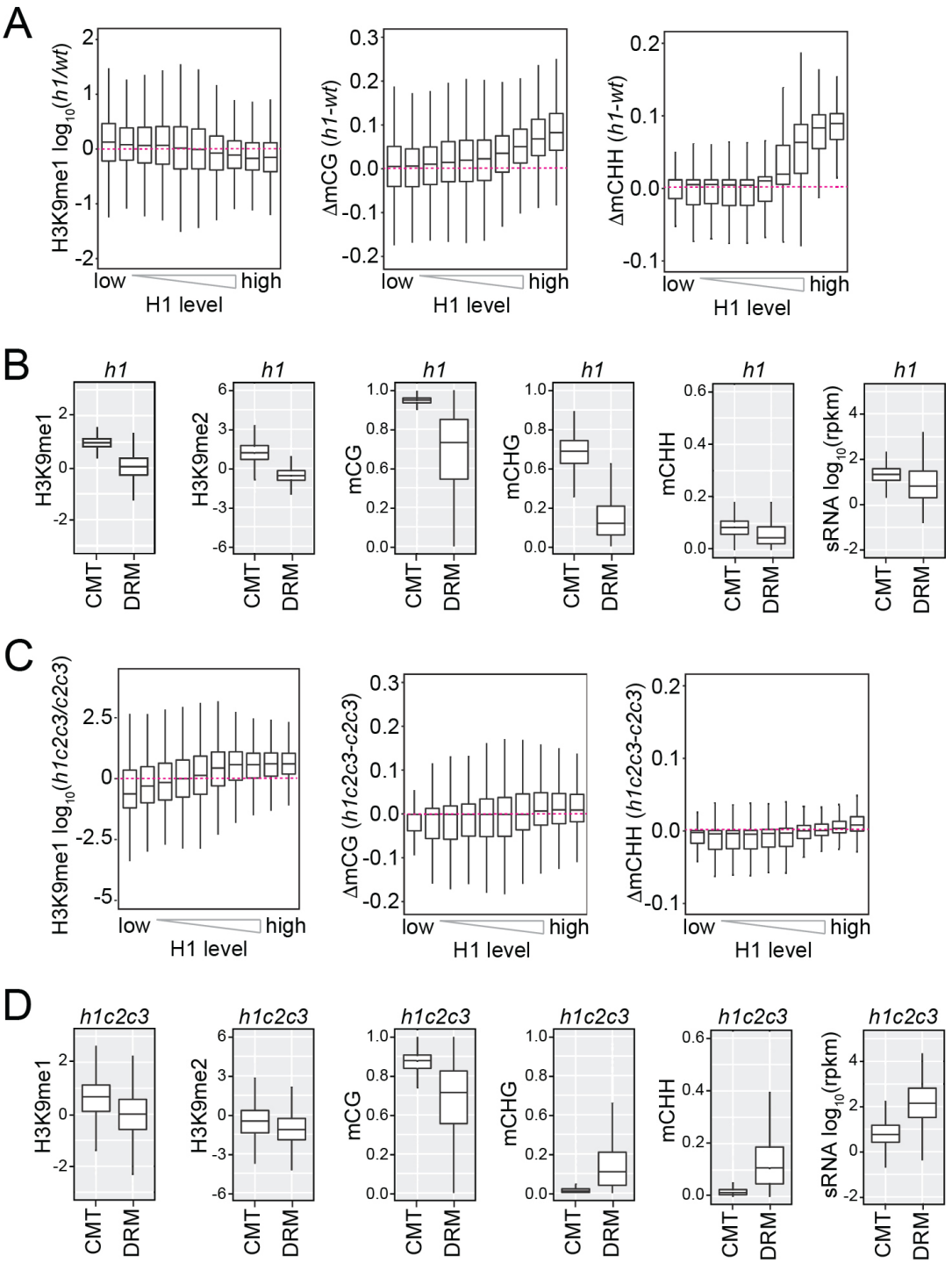

360 **Figure S7** H3K9 methylation, DNA methylation and sRNA expression in *h1* and *h1c2c3* plants.

361 **(A** and **C)** Boxplots of H3K9me1, mCG and mCHH methylation change in *h1* vs. *wt* (**A**) and

362 *h1c2c3* vs. *c2c3* (**C**). **(B** and **D)** Boxplots of H3K9 methylation, DNA methylation, and sRNA

363 expression levels at CMT and DRM TEs in *h1* plants (**B**) and *h1c2c3* plants (**D**).

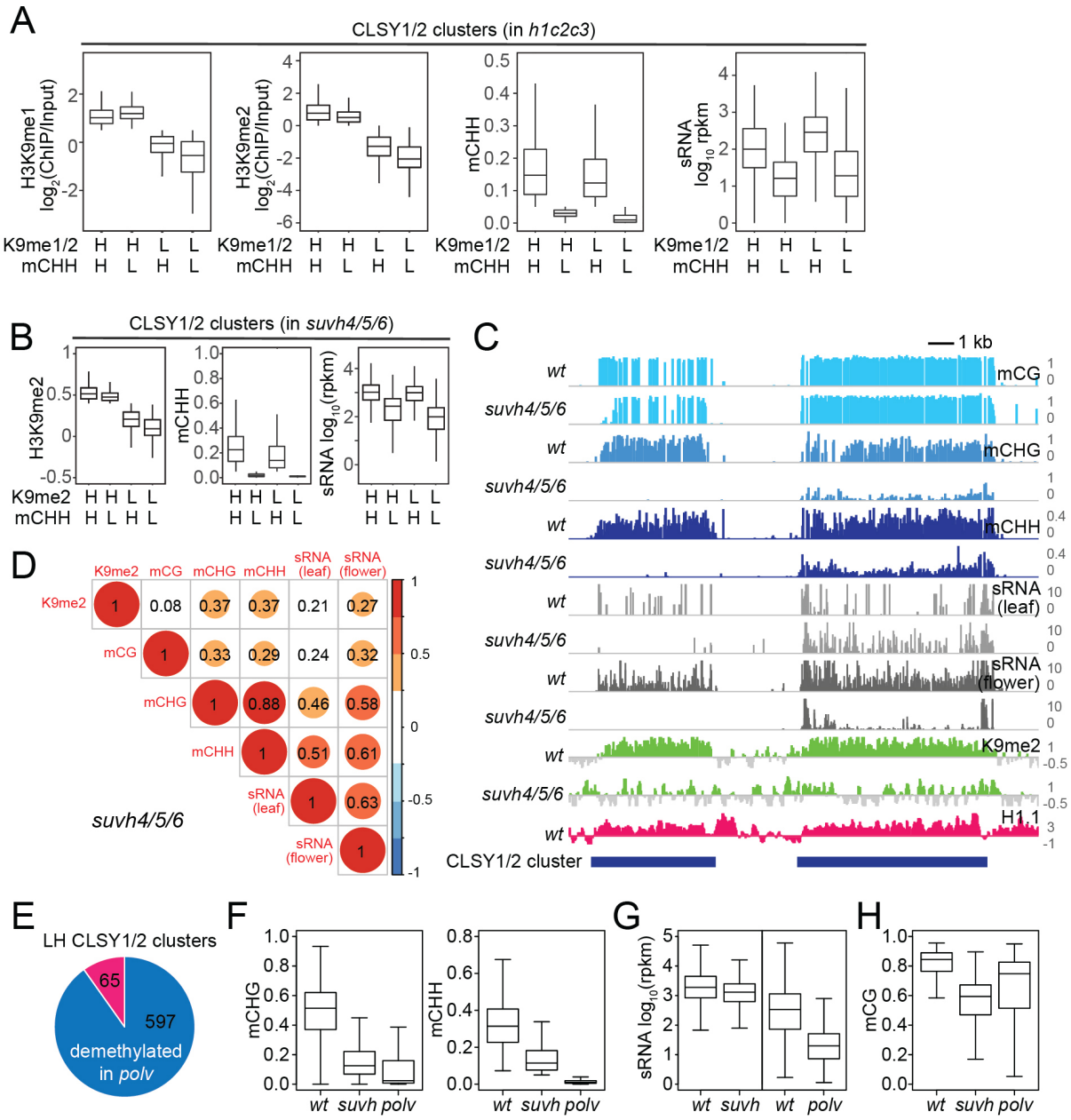

364 **Figure 8** CLSY1/2-dependent sRNA expression is associated with non-CG methylation.

365 **(A)** Boxplots of H3K9me1, H3K9me2, mCHH and sRNA expression levels at CLSY1/2-

366 dependent sRNA clusters in *h1c2c3* plants. sRNA clusters were classified by H3K9

367 methylation level (H3K9me1>0.5, H3K9me2>0 as high H3K9me (H), and the rest as low

368 H3K9me (L)) and mCHH level (mCHH>0.05 as high mCHH (H) and the rest as low mCHH

369 (L)). **(B)** Boxplots of H3K9me2, mCHH and sRNA expression levels at CLSY1/2-dependent

370 sRNA clusters in *suvh4/5/6* plants. sRNA clusters were classified by H3K9me2 level

371 (H3K9me2>0 as high H3K9me2 (H) and the rest as low H3K9me2 (L)) and mCHH level as in

(**A**). **(C)** Examples of CLSY1/2 sRNA clusters with high H3K9me2 *in suvh4/5/6* but different non-CG methylation levels (Chr1:17,520,000-17,538,000). **(D)** Correlation among H3K9me2, DNA methylation, and sRNA expression in *suvh456* plants. **(E)** Overlap between H3K9me2 low/mCHH high CLSY1/2 clusters (LH) in *suvh4/5/6* plants and mCHH demethylated CLSY1/2 clusters in *polv* plants. **(F-H)** Boxplots of non-CG methylation levels (**F**), sRNA expression (**G**), and mCG levels (**H**) at 597 CLSY1/2 clusters that lose mCHH in *plov* (blue in panel E).

CLSY1/2 RdDM activity specifically associates with non-CG methylation

24-nt sRNA expression is globally associated with non-CG methylation rather than H3K9me in *h1c2c3*, but these correlations are primarily driven by heterochromatic regions with low *wt* RdDM. To determine if this trend translates to euchromatic TEs where SHH1 is required for RdDM, we analyzed associations between H3K9me, DNA methylation, and sRNA expression in published CLSY1/2 sRNA clusters in *wt* plants (Figure 8A) (Zhou et al., 2018). In clusters grouped by H3K9me and mCHH, sRNA expression is associated with high mCHH, but not with high H3K9me (Figure 8A), supporting the idea that non-CG methylation dictates Pol IV localization.

As a further test of our hypothesis, we analyzed published data from plants lacking the three H3K9 methyltransferases implicated in the CMT/SUVH positive feedback loop. In these *suvh4/5/6* mutants, H3K9me2 and non-CG methylation are strongly diminished and sRNA expression of CLSY1/2 clusters is decreased (Stroud et al., 2014; Zhou et al., 2018). If H3K9me2 recruits Pol IV via SHH1, the limited remaining H3K9me would be expected to correlate with sRNA. Instead, we find sRNA expression in *suvh4/5/6* follows mCHH but not H3K9me2 (Figure 8B-C, compare left and right elements in 8C), consistent with our observations in heterochromatin. 24-nt sRNA correlates much more strongly with non-CG

methylation than with H3K9me2 in *suvh4/5/6* plants (Figure 8D), highlighting the limited importance of H3K9me for sRNA biogenesis.

Finally, we assayed CLSY1/2 clusters with low *wt* H3K9me2 but high *wt* sRNA and mCHH (LH CLSY1/2 clusters) in *polv* mutants to determine whether non-CG methylation is required to maintain sRNA expression. RNA Pol V is not directly involved in sRNA production, but is an essential RdDM component required for DNA methylation because it recruits DRM2 (Erdmann and Picard, 2020; Matzke and Mosher, 2014; Raju et al., 2019; Wendte and Pikaard, 2017). 90% of the 662 LH CLSY1/2 clusters lose mCHH in *polv* plants (mCHH<0.05, Figure 8E), and the overall non-CG methylation of LH CLSY1/2 clusters is greatly reduced without Pol V (Figure 8F). In *suv4/5/6* mutants, LH CLSY1/2 clusters maintain sRNA expression, whereas sRNA expression in *polv* mutants is greatly reduced (Figure 8G). Furthermore, mCG at LH CLSY1/2 clusters is higher in *polv* than in *suvh4/5/6* plants (Figure 8H). Therefore, sRNA biogenesis is not sensitive to the loss of either H3K9me2 or mCG and specifically requires non-CG methylation.

Discussion

We have examined intertwined chromatin features – sRNA production, DNA methylation, and H3K9 methylation – to understand how the genomic sites of Pol IV activity are specified. We find that two main factors are involved. First, linker histone H1 prevents sRNA production in heterochromatin (Figure 9). Without H1, RdDM relocates from its usual euchromatic targets into heterochromatic TEs (Figure 1 and Figure S1), as has been recently observed by an independent study (Papareddy et al., 2020). Another heterochromatic protein, the histone variant H2A.W, may also contribute to the exclusion of RdDM from heterochromatin, but this effect is modest and only observed when H1 is absent (Bourguet et al., 2021). In the presence of H1, lack of H2A.W instead strengthens the exclusion of RdDM from heterochromatin,

potentially due to enhanced heterochromatic H1 accumulation (Bourguet et al., 2021). Overall, the available evidence indicates that H1 is the major factor excluding Pol IV from heterochromatin.

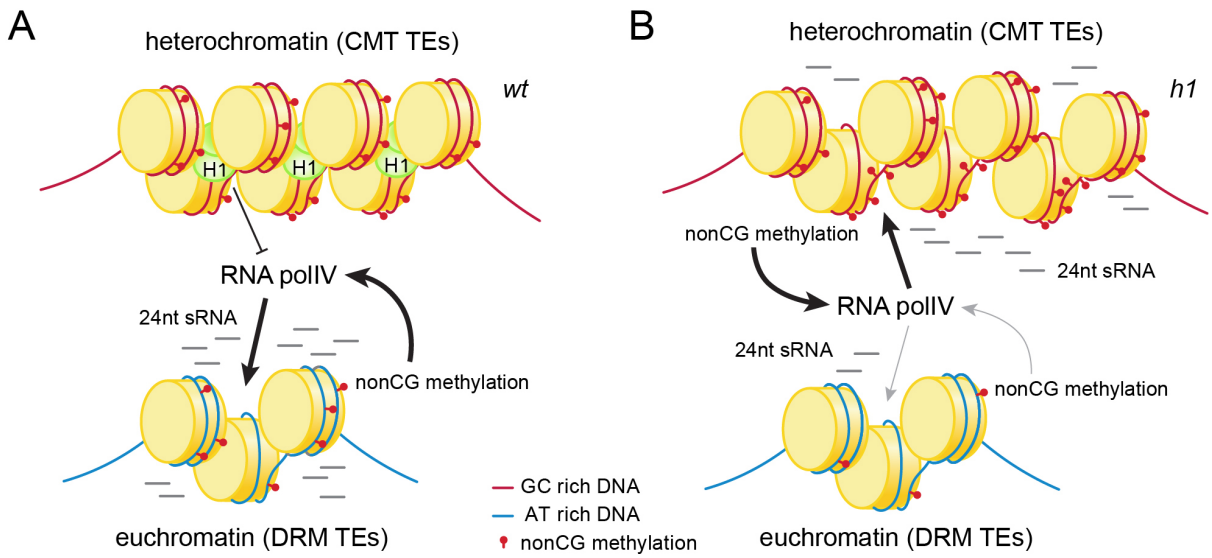

Figure 9 Histone H1 prevents non-CG methylation-mediated small RNA biogenesis in *Arabidopsis* heterochromatin.

(A) In *wt* plants, H1 binds to GC-rich CMT TEs to restrict access of RNA polymerase IV (pol IV). Pol IV binds to DRM TEs and produces sRNA. **(B)** In *h1* plants, RNA pol IV can transcribe non-CG methylated CMT TEs to produce 24-nt sRNA, which leads to DNA methylation of CMT TEs and reduced activity at DRM TEs.

Second, we find that non-CG methylation promotes Pol IV activity (Figure 9), contrary to the well-established view that Pol IV is recruited by H3K9me (Erdmann and Picard, 2020; Law et al., 2013; Raju et al., 2019; Wendte and Pikaard, 2017; Zhang et al., 2013), and the more recent proposal that mCG may be involved (Zhou et al., 2018). The hypothesis that non-CG methylation recruits Pol IV has a long history (Herr et al., 2005; Li et al., 2020; Zemach et al., 2013), but testing it has been challenging because non-CG methylation is associated with

435 other epigenetic and chromatin features, including mCG and H3K9me (Law and Jacobsen,
436 2010; Xu and Jiang, 2020; H. Zhang et al., 2018). The link with H3K9me has been particularly
437 difficult to break because of the CMT-SUVH feedback loop (Du et al., 2012; Johnson et al.,
438 2007; Li et al., 2018; Stoddard et al., 2019).

439 However, we have used *h1c2c3*, *suvh4/5/6* and *polv* mutants to disentangle H3K9me
440 and non-CG methylation. In all three backgrounds, sRNA biogenesis follows non-CG
441 methylation instead of H3K9me (Figure 7, 8 and Figure S7). The *h1c2c3* line has been
442 particularly informative due to the many TEs that maintain H3K9me but lack non-CG
443 methylation (Figure 7 and Figure S7). H3K9me may be substantially retained in *h1c2c3*
444 heterochromatin because lack of H1 allows SUVH methyltransferases easier access, so that the
445 weak affinity of their SRA domains for mCG suffices for effective recruitment (Johnson et al.,
446 2007; Li et al., 2018; Rajakumara et al., 2011). Whatever the mechanism, the strong linear
447 association between sRNA biogenesis and non-CG methylation, and the lack of such an
448 association with H3K9me and mCG (Figure 7 and 8), provide strong support for the hypothesis
449 that non-CG methylation recruits Pol IV (Figure 9).

450 The linking of Pol IV activity to non-CG methylation instead of H3K9me resolves
451 several thorny issues. First, the observation that SHH1 – the proposed H3K9me reader – is
452 preferentially required for RdDM where H3K9me is low (Zhou et al., 2018) can be easily
453 accommodated if H3K9me is not directly involved in RdDM. Similarly, the finding that severe
454 loss of H3K9me in *suvh4/5/6* mutants is accompanied by only a modest reduction of sRNA
455 levels (Zhou et al., 2018) is no longer mysterious. At a more fundamental level, this hypothesis
456 ties RdDM in a feedback loop with its product and unties it from a histone modification
457 produced by the distinct CMT-SUVH pathway and depleted from RdDM target sequences.
458 Breaking RdDM from dependence on any histone modification is also conceptually important
459 because a core theoretical strength of RdDM is the ability to maintain methylation at much

shorter sequences than those where stable histone-based epigenetic inheritance is possible (Angel et al., 2011; Lövkvist and Howard, 2021; Ramachandran and Henikoff, 2015; Zilberman and Henikoff, 2004).

Long TEs that can be effectively silenced by the histone-dependent CMT-SUVH pathway tend to be relatively GC-rich because they contain coding sequences (Sequeira-Mendes et al., 2014; To et al., 2020; Zemach et al., 2013). In contrast, short non-autonomous TEs and TE remnants tend to lack coding sequences and are thus AT-rich. In this context, the GC sequence preference of *Arabidopsis* H1 (Choi et al., 2020) may be key. GC bias is far from a H1 universal, with most animal H1 variants preferring AT-rich DNA (Cao et al., 2013; Izaurralde et al., 1989; Tomaszewski and Jerzmanowski, 1997). The preferences of plant H1 may have evolved, at least in part, to target it to coding sequences, including those of autonomous heterochromatic TEs. This would allow H1 to exclude RdDM from such sequences, which can cover vast tracts of plant genomes (Michael, 2014; Suzuki and Bird, 2008), and focus RdDM on the short TEs it is specialized to silence. The interplay of H1 and non-CG methylation can thus produce the preferential activity of RdDM at short, AT-rich TEs observed throughout flowering plants (Gouil and Baulcombe, 2016; Numa et al., 2015; Tan et al., 2018).

Methods

Biological materials

cmt2 and *cmt2cmt3* (Stroud et al., 2014; Zemach et al., 2013) plants were crossed to *h1.1h1.2* (Zemach et al., 2013) plants to generate *h1cmt2* and *h1cmt2cmt3* plants. To establish the *h1cmt2shh1* mutant line, we crossed *h1+/-cmt2* plants with *shh1* (SALK_074540C) plants, then isolated *h1cmt2shh1* homozygous siblings. *met1, h1met1, ddm1, h1ddm1* plants were described previously (Choi et al., 2020; Lyons and Zilberman, 2017). *Arabidopsis thaliana* seedlings were germinated and grown for 4-5 weeks on soil at 20-25℃ in growth chambers (16 hr day/8 hr night) for all the experiments performed except for *met1, h1met1*, and corresponding *wt* seedling sRNA libraries. These seedlings were germinated and grown for two weeks in half-strength Gamborg's B-5 liquid media (Caisson Labs, cat. No. GBP07) at 22-25℃ under continuous light with shaking at 125 RPM.

Bisulfite Sequencing (BS-seq) library preparation

BS-seq libraries were constructed using genomic DNA (gDNA) extracted from rosette leaves of 4-5-week-old plants. 500 ng total gDNA was sheared to 100-1000bp using Bioruptor Pico (Diagenode), then purified with 1.2X volume of SPRI beads (Beckman Coulter, cat. No. A63881). Fragmented gDNA was ligated to NEBNext Adaptor for Illumina using NEBNext Ultra II DNA library prep kit for Illumina (New England Biolabs, cat. No. E7645). We performed bisulfite conversion twice with ligated libraries (QIAGEN, cat. No. 59104) to prevent incomplete conversion (<99% conversion) of unmethylated cytosines. Converted libraries were subjected to SPRI bead purification with 0.8X volume of beads. We amplified bisulfite-converted libraries with NEB next indexing primers (New England Biolabs Inc. cat. No. E7335S).

Small RNA sequencing library preparation

To isolate small RNA, we extracted total RNA from rosette leaves of 4-5-week-old plants using Trizol (Invitrogen, cat. No. 15596026) according to manufacturer's manual. To remove DNA from samples, 5 µg of RNA was treated with DNA-free DNA removal kit (Thermo, cat. No. AM1907). 1 µg of DNA-free total RNA was subjected to sRNA library construction according to manufacturer's protocol (Illumina, cat. No. RS-200-0012 and RS-200-0024).

Native Chromatin Immunoprecipitation and sequencing library preparation

MNase digestion of native chromatin was carried out on 0.5g of 4 week old *Arabidopsis* rosette leaves as described previously (Lyons and Zilberman, 2017). Digestion was stopped with EGTA and chromatin was rotated at 4℃ for 30 minutes. The preparation was then centrifuged for 10 minutes at 2000 RPM and solubilized chromatin fragments were isolated by aspirating supernatant immediately. Chromatin was then diluted to 1ml in wash buffer A (50mM Tris-HCl pH 7.5, 50mM NaCl, 10mM EDTA) and antibody added at 1µl per 0.1 g of total starting material. Dilute Tween-20 was added to a final concentration of 0.1%, and the mixture was rotated overnight at 4℃. All buffers were supplemented with PMSF and protease inhibitor (Roche (Merck), cat. No. 11873580001). A standard immunoprecipitation procedure was used the following day. Briefly, pre-blocked Protein-A and -G dynabeads (Invitrogen, cat. No. 10001D and 10003D) were incubated with the chromatin preparation for 3 hrs. rotating at 4℃, and the beads/chromatin mixture was then washed on ice in Tris-EDTA buffer with increasing concentrations of NaCl, starting at 50mM and ending at 150mM. DNA was eluted from beads by shaking in 1% SDS and 1% NaHCO3 for 10 minutes at 55℃, and DNA was purified with phenol-chloroform extraction. Input and ChIP DNA was converted into sequencing libraries using Celero DNA reagents (Tecan, cat. No. 3460-24) following manufacturer's instructions.

Sequencing

Sequencing was performed at the John Innes Centre with the NextSeq 500 (Ilumina), except for sRNA libraries from seedlings (*wt, met1,* and *h1met1*). These seedling libraries were sequenced at the Vincent J. Coates Genomic Sequencing Laboratory at the University of California, Berkeley with the HiSeq 4000 (Illumina).

Sequence Alignment and data preparation

For sRNA-seq libraries, adapter sequences were removed from reads using cutadapt (Martin, 2011). 18-28 bp, 21nt, and 24 nt fragments were isolated using the following cutadapt options: -m 18 -M 28, -m 21 -M 21, -m 24 -M 24. Reads were mapped with Bowtie (Langmead et al., 2009) allowing up to 1 mismatch and up to 10 multi-mapped reads. Aligned 21-nt or 24-nt read counts were normalized by reads per kilobase per million mapped reads (RPKM) of 18-28 bp fragments. ChIP-seq libraries were mapped with Bowtie (Langmead et al., 2009) allowing up to 2 mismatches and up to 10 multi-mapped reads. To calculate enrichment, ChIP samples were divided by input samples and transformed into $\log_2$ ratio values using deepTools2 bamCompare. For H3K9me1 and H3K9me2 from WT, *h1*, *ddm1*, *h1ddm1*, *c2c3*, and *h1c2c3*, we used a random subset of input reads equivalent to 25% of the total uniquely mapped reads of the corresponding IP for input into bamCompare. For BS-seq libraries, reads were mapped with the bs-sequel pipeline (https://zilbermanlab.net/tools/).

Description of *Arabidopsis* genome features

'Transposable elements' include transposon annotation from (Panda and Slotkin, 2020). Araport11 TE genes and pseudogenes, and genomic regions with TE-like DNA methylation (Cheng et al., 2017; Choi et al., 2020; Panda and Slotkin, 2020; Shahzad et al., 2021). We filtered out elements shorter than 250 bp. Previously, we merged overlapping TE annotations

into single TE unit, then defined heterochromatic TEs and euchromatic TEs as transposons that have more than 0 or less than 0 H3K9me2 (log_2 ChIP/Input) in *wt* plants (Choi et al., 2020). Both CMT and DRMs target these merged, long TEs, as the edges of TEs are methylated by DRMs and the bodies of TEs are methylated by CMTs. Therefore, to isolate TEs with non-CG methylation dependent on CMTs or DRMs, we did not merge TE annotations here. Among TEs with mCHH methylation (mCHH > 0.05), CMT-dependent TEs were defined as the TEs that lost mCHH methylation in *cmt2cmt3* plants (mCHH < 0.02 in *cmt2cmt3*). DRM-dependent TEs were defined as the TEs that lost mCHH methylation in *drm1drm2* plants (mCHH < 0.02 in *drm1drm2*). sRNA cluster annotation is from (Zhou et al., 2018).

Classification of MET1-dependent and -independent CMT TEs

We previously defined MET1-dependent TEs as the TEs that lost H3K9me2 in *met1* plants (Choi et al., 2020). In this study, to evaluate how DNA methylation affects CLSY3/4-dependent sRNA expression, we defined MET1-dependent TEs as the TEs that lost mCHH methylation in *met1* (mCHH in *wt* ≧ 0.05, mCHH in *met1* <0.05), and MET1-independent TEs as ones that keep mCHH methylation in *met1* (mCHH in *wt* ≧ 0.05, mCHH in *met1* ≧ 0.05).

Random forest classification and prediction

To measure the importance of each genetic and epigenetic marker to classify DRM and CMT TEs, we first calculated average enrichment of various histone modifications, histone H1, average sRNA expression and DNA methylation level at each TE using window_by_annotation.pl Perl script (https://zilbermanlab.net/tools/). We also included density of various cytosine sequence contexts. The importance of each variable was evaluated using 'randomForest' and 'measure_importance' function in RandomForestExplainer R package (Ishwaran et al., 2010). The importance matrices were visualized by 'plot_multi_way_importance' function of the same package.

To evaluate the predictive power of each variable, we randomly divided TEs into training and validation sets. The random forest classifier was built using TEs in the training set with indicated variables and the classification of each TE (DRM or CMT). The trained model was used to predict the category of TEs in the validation set, and the error rate was calculated by comparing the predicted classification and its actual classification. We used 'randomforest' and 'predict' function in randomForest R Package.

Data visualization

Enrichment scores of various genomic and epigenomic features were generated by window_by_annotation.pl Perl scripts (https://zilbermanlab.net/tools/). For scatter plots and heatscatter plots in Figure 1, the enrichment scores were imported to R (Davey et al., 1997) and visualized by ggplot2 R package (Wickham, 2009) or 'heatscatter' function in LSD R package (Venables and Ripley, 2002). For scatter plots and heatscatter plots in other figures, TEs were sorted by their GC content, then average feature enrichments of 100 TEs were calculated to reduce the variability of data. DNA methylation, H3K9 methylation and sRNA distribution around TEs were generated with ends_analysis.pl and average_ends_new.pl Perl scripts (https://zilbermanlab.net/tools/). For sRNA distribution, we removed bins with higher than 200 rpkm to prevent outliers skewing the average. For proportional Venn diagram, TE ID lists in each group were uploaded to BioVenn (Hulsen et al., 2008). To visualize the relationship among genetic, epigenetic features and sRNA expression in *c2c3* and *h1c2c3* plants, principal component analysis was applied to arrays of features using Gene Cluster 3.0 (de Hoon et al., 2004; Figure 6C). For Pearson's correlation coefficient plots, the DNA methylation, H3K9 methylation, and sRNA expression level matrices were imported to R and visualized using corrplot R package (Friendly, 2002; Murdoch and Chow, 1996; Figure 7 and 8). Screenshots of *Arabidopsis* genomic loci were taken in IGV (Robinson et al., 2011;

Thorvaldsdottir et al., 2013). Treeview was used to generate heatmaps (de Hoon et al., 2004). For sRNA plots around nucleosomes (Figure 2), previously published nucleosome dyad coordinates were used (Lyons and Zilberman 2017) as anchors around which 10-bp bins of 24-nt sRNA were averaged and plotted. Autocorrelation estimates were generated on these averages using the built-in R 'acf' function.

Use of Previously Published Data

DNA methylation data of *c2c3* and *ddcc* plants (Stroud et al., 2014), DNA methylation and sRNA data of *clsy1/2, clsy3/4,* and *shh1* plants (Zhou et al., 2018), DNA methylation and H3K9me data of *met1* and *h1met1* plants (Choi et al., 2020), DNA methylation, H3K9me2, and sRNA expression data of *suvh4/5/6* plants (Papareddy et al., 2020; Stroud et al., 2014), and DNA methylation and sRNA data of *polv* plants (Johnson et al., 2014; Zhong et al., 2012) were obtained through GEO (GEO accessions: GSE51304, GSE99694, GSE122394, GSE152971, GSE52041 and GSE39247).

Data Availability

The accession number for the NGS data reported in this paper is GEO: GSEXXXXXX.

610 **References**

611 Allshire RC, Madhani HD. 2018. Ten principles of heterochromatin formation and function.
612 *Nat Rev Mol Cell Biol* **19**:229–244. doi:10.1038/nrm.2017.119
613 Angel A, Song J, Dean C, Howard M. 2011. A Polycomb-based switch underlying
614 quantitative epigenetic memory. *Nature* **476**:105–108. doi:10.1038/nature10241
615 Berry S, Dean C. 2015. Environmental perception and epigenetic memory: Mechanistic
616 insight through FLC. *Plant J* **83**:133–148. doi:10.1111/tpj.12869
617 Blevins T, Podicheti R, Mishra V, Marasco M, Wang J, Rusch D, Tang H, Pikaard CS. 2015.
618 Identification of Pol IV and RDR2-dependent precursors of 24 nt siRNAs guiding de
619 novo DNA methylation in Arabidopsis. *Elife* **4**:e09591. doi:10.7554/eLife.09591
620 Bourguet P, Picard CL, Yelagandula R, Pélissier T, Lorković ZJ, Feng S, Pouch-Pélissier M-
621 N, Schmücker A, Jacobsen SE, Berger F, Mathieu O. 2021. The histone variant H2A.W
622 and linker histone H1 co-regulate heterochromatin accessibility and DNA methylation.
623 *Nat Commun* **12**:2683. doi:10.1038/s41467-021-22993-5
624 Bourque G, Burns KH, Gehring M, Gorbunova V, Seluanov A, Hammell M, Imbeault M,
625 Izsvák Z, Levin HL, Macfarlan TS, Mager DL, Feschotte C. 2018. Ten things you
626 should know about transposable elements. *Genome Biol* **19**:199. doi:10.1186/s13059-
627 018-1577-z
628 Breiman L. 2001. Random forests. *Mach Learn* **45**:5–32. doi:10.1023/A:1010933404324
629 Cao K, Lailler N, Zhang Y, Kumar A, Uppal K, Liu Z, Lee EK, Wu H, Medrzycki M, Pan C,
630 Ho P-Y, Cooper GP, Dong X, Bock C, Bouhassira EE, Fan Y. 2013. High-resolution
631 mapping of H1 linker histone variants in embryonic stem cells. *PLoS Genet* **9**:e1003417.
632 doi:10.1371/journal.pgen.1003417
633 Cheng C-Y, Krishnakumar V, Chan AP, Thibaud-Nissen F, Schobel S, Town CD. 2017.
634 Araport11: a complete reannotation of the Arabidopsis thaliana reference genome. *Plant*

635 *J* **89**:789–804. doi:10.1111/tpj.13415

636 Choi J, Lyons DB, Kim MY, Moore JD, Zilberman D. 2020. DNA methylation and histone
637 H1 jointly repress transposable elements and aberrant intragenic transcripts. *Mol Cell*
638 **77**:310-323.e7. doi:10.1016/j.molcel.2019.10.011

639 Cokus SJ, Feng S, Zhang X, Chen Z, Merriman B, Haudenschild CD, Pradhan S, Nelson SF,
640 Pellegrini M, Jacobsen SE. 2008. Shotgun bisulphite sequencing of the Arabidopsis
641 genome reveals DNA methylation patterning. *Nature* **452**:215–219.
642 doi:10.1038/nature06745

643 Davey C, Pennings S, Allan J. 1997. CpG methylation remodels chromatin structure in vitro.
644 *J Mol Biol* **267**:276–288. doi:10.1006/JMBI.1997.0899

645 de Hoon MJL, Imoto S, Nolan J, Miyano S. 2004. Open source clustering software.
646 *Bioinformatics* **20**:1453–1454. doi:10.1093/bioinformatics/bth078

647 Deleris A, Stroud H, Bernatavichute Y, Johnson E, Klein G, Schubert D, Jacobsen SE. 2012.
648 Loss of the DNA methyltransferase MET1 induces H3K9 hypermethylation at PcG
649 target genes and redistribution of H3K27 trimethylation to transposons in Arabidopsis
650 thaliana. *PLoS Genet* **8**:e1003062. doi:10.1371/journal.pgen.1003062

651 Du J, Johnson LM, Groth M, Feng S, Hale CJ, Li S, Vashisht AA, Gallego-Bartolome J,
652 Wohlschlegel JA, Patel DJ, Jacobsen SE. 2014. Mechanism of DNA methylation-
653 directed histone methylation by KRYPTONITE. *Mol Cell* **55**:495–504.
654 doi:10.1016/j.molcel.2014.06.009

655 Du J, Zhong X, Bernatavichute Y V., Stroud H, Feng S, Caro E, Vashisht AA, Terragni J,
656 Chin HG, Tu A, Hetzel J, Wohlschlegel JA, Pradhan S, Patel DJ, Jacobsen SE. 2012.
657 Dual binding of chromomethylase domains to H3K9me2-containing nucleosomes
658 directs DNA methylation in plants. *Cell* **151**:167–180. doi:10.1016/j.cell.2012.07.034

659 Erdmann RM, Picard CL. 2020. RNA-directed DNA methylation, *PLoS Genet.* **16**,

660 e1009034. doi:10.1371/journal.pgen.1009034

661 Feng S, Cokus SJ, Zhang X, Chen P-Y, Bostick M, Goll MG, Hetzel J, Jain J, Strauss SH,
662 Halpern ME, Ukomadu C, Sadler KC, Pradhan S, Pellegrini M, Jacobsen SE. 2010.
663 Conservation and divergence of methylation patterning in plants and animals. *Proc Natl*
664 *Acad Sci USA* **107**:8689–8694. doi:10.1073/pnas.1002720107

665 Feng W, Michaels SD. 2015. Accessing the inaccessible: The organization, transcription,
666 replication, and repair of heterochromatin in plants. *Annu Rev Genet* **49**:439–459.
667 doi:10.1146/annurev-genet-112414-055048

668 Friendly M. 2002. Corrgrams: Exploratory displays for correlation matrices. *Am Stat* **56**:316–
669 324. doi:10.1198/000313002533

670 Gouil Q, Baulcombe DC. 2016. DNA methylation signatures of the plant
671 chromomethyltransferases. *PLoS Genet* **12**:e1006526.
672 doi:10.1371/journal.pgen.1006526

673 Greenberg MVC, Deleris A, Hale CJ, Liu A, Feng S, Jacobsen SE. 2013. Interplay between
674 active chromatin marks and RNA-directed DNA methylation in Arabidopsis thaliana.
675 *PLoS Genet* **9**:e1003946. doi:10.1371/journal.pgen.1003946

676 Herr AJ, Jensen MB, Dalmay T, Baulcombe DC. 2005. RNA polymerase IV directs silencing
677 of endogenous DNA. *Science* **308**:118–120. doi:10.1126/science.1106910

678 Hulsen T, de Vlieg J, Alkema W. 2008. BioVenn – a web application for the comparison and
679 visualization of biological lists using area-proportional Venn diagrams. *BMC Genomics*
680 **9**:488. doi:10.1186/1471-2164-9-488

681 Ishwaran H, Kogalur UB, Gorodeski EZ, Minn AJ, Lauer MS. 2010. High-dimensional
682 variable selection for survival data. *J Am Stat Assoc* **105**:205–217.
683 doi:10.1198/jasa.2009.tm08622

684 Ito T, Tarutani Y, To TK, Kassam M, Duvernois-Berthet E, Cortijo S, Takashima K, Saze H,

685 Toyoda A, Fujiyama A, Colot V, Kakutani T. 2015. Genome-wide negative feedback
686 drives transgenerational DNA methylation dynamics in Arabidopsis. *PLoS Genet*
687 **11**:e1005154. doi:10.1371/journal.pgen.1005154
688 Izaurralde E, Käs E, Laemmli UK. 1989. Highly preferential nucleation of histone H1
689 assembly on scaffold-associated regions. *J Mol Biol* **210**:573–585.
690 doi:https://doi.org/10.1016/0022-2836(89)90133-2
691 Johnson LM, Bostick M, Zhang X, Kraft E, Henderson I, Callis J, Jacobsen SE. 2007. The
692 SRA methyl-cytosine-binding domain links DNA and histone methylation. *Curr Biol*
693 **17**:379–384. doi:https://doi.org/10.1016/j.cub.2007.01.009
694 Johnson LM, Du J, Hale CJ, Bischof S, Feng S, Chodavarapu RK, Zhong X, Marson G,
695 Pellegrini M, Segal DJ, Patel DJ, Jacobsen SE. 2014. SRA- and SET-domain-containing
696 proteins link RNA polymerase V occupancy to DNA methylation. *Nature* **507**:124–128.
697 doi:10.1038/nature12931
698 Kim MY, Zilberman D. 2014. DNA methylation as a system of plant genomic immunity.
699 *Trends Plant Sci* **19**:320–326. doi:10.1016/j.tplants.2014.01.014
700 Langmead B, Trapnell C, Pop M, Salzberg SL. 2009. Ultrafast and memory-efficient
701 alignment of short DNA sequences to the human genome. *Genome Biol* **10**:R25.
702 doi:10.1186/gb-2009-10-3-r25
703 Law JA, Du J, Hale CJ, Feng S, Krajewski K, Palanca AMS, Strahl BD, Patel DJ, Jacobsen
704 SE. 2013. Polymerase IV occupancy at RNA-directed DNA methylation sites requires
705 SHH1. *Nature* **498**:385–389. doi:10.1038/nature12178
706 Law JA, Jacobsen SE. 2010. Establishing, maintaining and modifying DNA methylation
707 patterns in plants and animals. *Nat Rev Genet* **11**:204–220. doi:10.1038/nrg2719
708 Li J, Yang D-L, Huang H, Zhang G, He L, Pang J, Lozano-Durán R, Lang Z, Zhu J-K. 2020.
709 Epigenetic memory marks determine epiallele stability at loci targeted by de novo DNA

methylation. *Nat Plants* **6**:661–674. doi:10.1038/s41477-020-0671-x

Li X, Harris CJ, Zhong Z, Chen W, Liu R, Jia B, Wang Z, Li S, Jacobsen SE, Du J. 2018. Mechanistic insights into plant SUVH family H3K9 methyltransferases and their binding to context-biased non-CG DNA methylation. *Proc Natl Acad Sci USA* **115**:E8793–E8802. doi:10.1073/pnas.1809841115

Lippman Z, Gendrel A-V, Black M, Vaughn MW, Dedhia N, Richard McCombie W, Lavine K, Mittal V, May B, Kasschau KD, Carrington JC, Doerge RW, Colot V, Martienssen R. 2004. Role of transposable elements in heterochromatin and epigenetic control. *Nature* **430**:471–476. doi:10.1038/nature02651

Lister R, O'Malley RC, Tonti-Filippini J, Gregory BD, Berry CC, Millar AH, Ecker JR. 2008. Highly integrated single-base resolution maps of the epigenome in Arabidopsis. *Cell* **133**:523–536. doi:10.1016/J.CELL.2008.03.029

Liu Z-W, Shao C-R, Zhang C-J, Zhou J-X, Zhang S-W, Li L, Chen S, Huang H-W, Cai T, He X-J. 2014. The SET domain proteins SUVH2 and SUVH9 are required for Pol V occupancy at RNA-directed DNA methylation loci. *PLoS Genet* **10**:e1003948. doi:10.1371/journal.pgen.1003948

Lövkvist C, Howard M. 2021. Using computational modelling to reveal mechanisms of epigenetic Polycomb control. *Biochem Soc Trans* **49**:71–77. doi:10.1042/BST20190955

Lyons DB, Zilberman D. 2017. DDM1 and Lsh remodelers allow methylation of DNA wrapped in nucleosomes. *Elife* **6**:e30674. doi:10.7554/eLife.30674

Martin M. 2011. Cutadapt removes adapter sequences from high-throughput sequencing reads. *EMBnet.journal* **17**:10–12. doi:10.14806/ej.17.1.200

Matzke MA, Mosher RA. 2014. RNA-directed DNA methylation: an epigenetic pathway of increasing complexity. *Nat Rev Genet* **15**:394–408. doi:10.1038/nrg3683

Michael TP. 2014. Plant genome size variation: bloating and purging DNA. *Brief Funct*

Genomics **13**:308–317. doi:10.1093/bfgp/elu005

Miura A, Nakamura M, Inagaki S, Kobayashi A, Saze H, Kakutani T. 2009. An Arabidopsis jmjC domain protein protects transcribed genes from DNA methylation at CHG sites. *EMBO J* **28**:1078–1086. doi:10.1038/emboj.2009.59

Murdoch DJ, Chow ED. 1996. A Graphical Display of Large Correlation Matrices. *Am Stat* **50**:178–180. doi:10.1080/00031305.1996.10474371

Niederhuth CE, Bewick AJ, Ji L, Alabady MS, Kim K Do, Li Q, Rohr NA, Rambani A, Burke JM, Udall JA, Egesi C, Schmutz J, Grimwood J, Jackson SA, Springer NM, Schmitz RJ. 2016. Widespread natural variation of DNA methylation within angiosperms. *Genome Biol* **17**:194. doi:10.1186/s13059-016-1059-0

Numa H, Yamaguchi K, Shigenobu S, Habu Y. 2015. Gene body CG and CHG methylation and suppression of centromeric CHH methylation are mediated by DECREASE IN DNA METHYLATION1 in rice. *Mol Plant* **8**:1560–1562. doi:10.1016/j.molp.2015.08.002

Osakabe A, Jamge B, Axelsson E, Montgomery SA, Akimcheva S, Kuehn AL, Pisupati R, Lorković ZJ, Yelagandula R, Kakutani T, Berger F. 2021. The chromatin remodeler DDM1 prevents transposon mobility through deposition of histone variant H2A.W. *Nat Cell Biol* **23**:391–400. doi:10.1038/s41556-021-00658-1

Panda K, Ji L, Neumann DA, Daron J, Schmitz RJ, Slotkin RK. 2016. Full-length autonomous transposable elements are preferentially targeted by expression-dependent forms of RNA-directed DNA methylation. *Genome Biol* **17**:170. doi:10.1186/s13059-016-1032-y

Panda K, Slotkin RK. 2020. Long-read cDNA sequencing enables a “gene-like” transcript annotation of transposable elements. *Plant Cell* **32**:2687–2698. doi:10.1105/tpc.20.00115

760 Papareddy RK, Páldi K, Paulraj S, Kao P, Lutzmayer S, Nodine MD. 2020. Chromatin
761 regulates expression of small RNAs to help maintain transposon methylome
762 homeostasis in Arabidopsis. *Genome Biol* **21**:251. doi:10.1186/s13059-020-02163-4
763 Rajakumara E, Law JA, Simanshu DK, Voigt P, Johnson LM, Reinberg D, Patel DJ,
764 Jacobsen SE. 2011. A dual flip-out mechanism for 5mC recognition by the Arabidopsis
765 SUVH5 SRA domain and its impact on DNA methylation and H3K9 dimethylation in
766 vivo. *Genes Dev* **25**:137–152. doi:10.1101/gad.1980311
767 Raju SKK, Ritter EJ, Niederhuth CE. 2019. Establishment, maintenance, and biological roles
768 of non-CG methylation in plants. *Essays Biochem* **63**:743–755.
769 doi:10.1042/EBC20190032
770 Ramachandran S, Henikoff S. 2015. Replicating nucleosomes. *Sci Adv* **1**:e1500587.
771 doi:10.1126/sciadv.1500587
772 Ritter EJ, Niederhuth CE. 2021. Intertwined evolution of plant epigenomes and genomes.
773 *Curr Opin Plant Biol* **61**:101990. doi:https://doi.org/10.1016/j.pbi.2020.101990
774 Robinson JT, Thorvaldsdóttir H, Winckler W, Guttman M, Lander ES, Getz G, Mesirov JP.
775 2011. Integrative genomics viewer. *Nat Biotechnol* **29**:24–26. doi:10.1038/nbt.1754
776 Rougée M, Quadrana L, Zervudacki J, Hure V, Colot V, Navarro L, Deleris A. 2020.
777 Polycomb mutant partially suppresses DNA hypomethylation-associated phenotypes in
778 Arabidopsis. *Life Sci Alliance* **4**:e202000848. doi:10.26508/lsa.202000848
779 Rutowicz K, Puzio M, Halibart-Puzio J, Lirski M, Kotliński M, Kroteń MA, Knizewski L,
780 Lange B, Muszewska A, Śniegowska-Świerk K, Kościelniak J, Iwanicka-Nowicka R,
781 Buza K, Janowiak F, Żmuda K, Jõesaar I, Laskowska-Kaszub K, Fogtman A, Kollist H,
782 Zielenkiewicz P, Tiuryn J, Siedlecki P, Swiezewski S, Ginalski K, Koblowska M,
783 Archacki R, Wilczynski B, Rapacz M, Jerzmanowski A. 2015. A specialized histone H1
784 variant is required for adaptive responses to complex abiotic stress and related DNA

785 methylation in Arabidopsis. *Plant Physiol* **169**:2080–2101. doi:10.1104/pp.15.00493

786 Sequeira-Mendes J, Aragüez I, Peiró R, Mendez-Giraldez R, Zhang X, Jacobsen SE, Bastolla
787 U, Gutierrez C. 2014. The functional topography of the Arabidopsis genome is
788 organized in a reduced number of linear motifs of chromatin states. *Plant Cell* **26**:2351–
789 2366. doi:10.1105/tpc.114.124578

790 Shahzad Z, Moore JD, Zilberman D. 2021. Gene body methylation mediates epigenetic
791 inheritance of plant traits. *bioRxiv* 2021.03.15.435374. doi:10.1101/2021.03.15.435374

792 Sigman MJ, Slotkin RK. 2016. The first rule of plant transposable element silencing:
793 Location, location, location. *Plant Cell* **28**:304–313. doi:10.1105/tpc.15.00869

794 Smith LM, Pontes O, Searle I, Yelina N, Yousafzai FK, Herr AJ, Pikaard CS, Baulcombe
795 DC. 2007. An SNF2 protein associated with nuclear RNA silencing and the spread of a
796 silencing signal between cells in Arabidopsis. *Plant Cell* **19**:1507–1521.
797 doi:10.1105/tpc.107.051540

798 Soppe WJJ, Jasencakova Z, Houben A, Kakutani T, Meister A, Huang MS, Jacobsen SE,
799 Schubert I, Fransz PF. 2002. DNA methylation controls histone H3 lysine 9 methylation
800 and heterochromatin assembly in Arabidopsis. *EMBO J* **21**:6549–6559.
801 doi:10.1093/emboj/cdf657

802 Stoddard CI, Feng S, Campbell MG, Liu W, Wang H, Zhong X, Bernatavichute Y, Cheng Y,
803 Jacobsen SE, Narlikar GJ. 2019. A nucleosome bridging mechanism for activation of a
804 maintenance DNA methyltransferase. *Mol Cell* **73**:73-83.e6.
805 doi:10.1016/J.MOLCEL.2018.10.006

806 Stroud H, Do T, Du J, Zhong X, Feng S, Johnson L, Patel DJ, Jacobsen SE. 2014. Non-CG
807 methylation patterns shape the epigenetic landscape in Arabidopsis. *Nat Struct Mol Biol*
808 **21**:64–72. doi:10.1038/nsmb.2735

809 Suzuki MM, Bird A. 2008. DNA methylation landscapes: Provocative insights from

epigenomics. *Nat Rev Genet* **9**:465–476. doi:10.1038/nrg2341

Tan F, Lu Y, Jiang W, Wu T, Zhang R, Zhao Y, Zhou D-X. 2018. DDM1 represses noncoding RNA expression and RNA-directed DNA methylation in heterochromatin. *Plant Physiol* **177**:1187–1197. doi:10.1104/pp.18.00352

Teixeira FK, Heredia F, Sarazin A, Roudier F, Boccara M, Ciaudo C, Cruaud C, Poulain J, Berdasco M, Fraga MF, Voinnet O, Wincker P, Esteller M, Colot V. 2009. A role for RNAi in the selective correction of DNA methylation defects. *Science* **323**:1600–1604. doi:10.1126/science.1165313

Thorvaldsdottir H, Robinson JT, Mesirov JP. 2013. Integrative Genomics Viewer (IGV): High-performance genomics data visualization and exploration. *Brief Bioinform* **14**:178–192. doi:10.1093/bib/bbs017

To TK, Nishizawa Y, Inagaki S, Tarutani Y, Tominaga S, Toyoda A, Fujiyama A, Berger F, Kakutani T. 2020. RNA interference-independent reprogramming of DNA methylation in Arabidopsis. *Nat Plants* **6**:1455–1467. doi:10.1038/s41477-020-00810-z

Tomaszewski R, Jerzmanowski A. 1997. The AT-rich flanks of the oocyte-type 5S RNA gene of Xenopus laevis act as a strong local signal for histone H1-mediated chromatin reorganization in vitro. *Nucleic Acids Res* **25**:458–465. doi:10.1093/nar/25.3.458

Venables WN, Ripley BD. 2002. Modern applied statistics with S. Springer.

Wendte JM, Pikaard CS. 2017. The RNAs of RNA-directed DNA methylation. *Biochim Biophys Acta - Gene Regul Mech* **1860**:140–148. doi:https://doi.org/10.1016/j.bbagrm.2016.08.004

Wickham H. 2009. Ggplot2 : Elegant graphics for data analysis. New York: Springer-Verlag.

Wongpalee SP, Liu S, Gallego-Bartolomé J, Leitner A, Aebersold R, Liu W, Yen L, Nohales MA, Kuo PH, Vashisht AA, Wohlschlegel JA, Feng S, Kay SA, Zhou ZH, Jacobsen SE. 2019. CryoEM structures of Arabidopsis DDR complexes involved in RNA-directed

DNA methylation. *Nat Commun* **10**:3916. doi:10.1038/s41467-019-11759-9

Xu L, Jiang H. 2020. Writing and reading histone H3 lysine 9 methylation in Arabidopsis. *Front. Plant Sci*. **11**:452. doi: 10.3389/fpls.2020.00452

Yaari R, Noy-Malka C, Wiedemann G, Gershovitz NA, Reski R, Katz A, Ohad N. 2015. DNA METHYLTRANSFERASE 1 is involved in mCG and mCCG DNA methylation and is essential for sporophyte development in Physcomitrella patens. *Plant Mol Biol* **88**:387–400. doi: 10.1007/s11103-015-0328-8

Yang D-L, Zhang G, Wang L, Li J, Xu D, Di C, Tang K, Yang L, Zeng L, Miki D, Duan C-G, Zhang H, Zhu J-K. 2018. Four putative SWI2/SNF2 chromatin remodelers have dual roles in regulating DNA methylation in Arabidopsis. *Cell Discov* **4**:55. doi:10.1038/s41421-018-0056-8

Zabet NR, Catoni M, Prischi F, Paszkowski J. 2017. Cytosine methylation at CpCpG sites triggers accumulation of non-CpG methylation in gene bodies. *Nucleic Acids Res* **45**:3777–3784. doi:10.1093/nar/gkw1330

Zemach A, Kim MY, Hsieh P-H, Coleman-Derr D, Eshed-Williams L, Thao K, Harmer SL, Zilberman D. 2013. The Arabidopsis nucleosome remodeler DDM1 allows DNA methyltransferases to access H1-containing heterochromatin. *Cell* **153**:193–205. doi:10.1016/j.cell.2013.02.033

Zemach A, McDaniel IE, Silva P, Zilberman D. 2010. Genome-wide evolutionary analysis of eukaryotic DNA methylation. *Science* **328**:916–919. doi:10.1126/science.1159151

Zhai J, Bischof S, Wang H, Feng S, Lee T-F, Teng C, Chen X, Park SY, Liu L, Gallego-Bartolome J, Liu W, Henderson IR, Meyers BC, Ausin I, Jacobsen SE. 2015. A one precursor one siRNA model for pol IV-dependent siRNA biogenesis. *Cell* **163**:445–55. doi:10.1016/j.cell.2015.09.032

Zhang H, Lang Z, Zhu J-K. 2018. Dynamics and function of DNA methylation in plants. *Nat*

Rev Mol Cell Biol **19**:489–506. doi:10.1038/s41580-018-0016-z

Zhang H, Ma ZY, Zeng L, Tanaka K, Zhang CJ, Ma J, Bai G, Wang P, Zhang SW, Liu ZW, Cai T, Tang K, Liu R, Shi X, He XJ, Zhu JK. 2013. DTF1 is a core component of RNA-directed DNA methylation and may assist in the recruitment of Pol IV. *Proc Natl Acad Sci USA* **110**:8290–8295. doi:10.1073/pnas.1300585110

Zhang Y, Harris CJ, Liu Q, Liu W, Ausin I, Long Y, Xiao L, Feng L, Chen Xu, Xie Y, Chen Xinyuan, Zhan L, Feng S, Li JJ, Wang H, Zhai J, Jacobsen SE. 2018. Large-scale comparative epigenomics reveals hierarchical regulation of non-CG methylation in Arabidopsis. *Proc Natl Acad Sci USA* E1069–E1074. doi:10.1073/pnas.1716300115

Zhong X, Hale CJ, Law JA, Johnson LM, Feng S, Tu A, Jacobsen SE. 2012. DDR complex facilitates global association of RNA polymerase V to promoters and evolutionarily young transposons. *Nat Struct Mol Biol* **19**:870–875. doi:10.1038/nsmb.2354

Zhou M, Palanca AMS, Law JA. 2018. Locus-specific control of the de novo DNA methylation pathway in Arabidopsis by the CLASSY family. *Nat Genet* **50**:865–873. doi:10.1038/s41588-018-0115-y

Zilberman D, Henikoff S. 2004. Silencing of transposons in plant genomes: Kick them when they're down. *Genome Biol* **5**:249. doi:10.1186/gb-2004-5-12-249